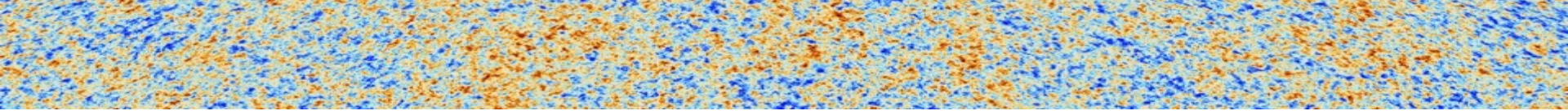

Primordial GW from CMB: observational perspective

Prof. Francesco Piacentini – Sapienza University of Rome

PhD Course, Nov 16th, 2021

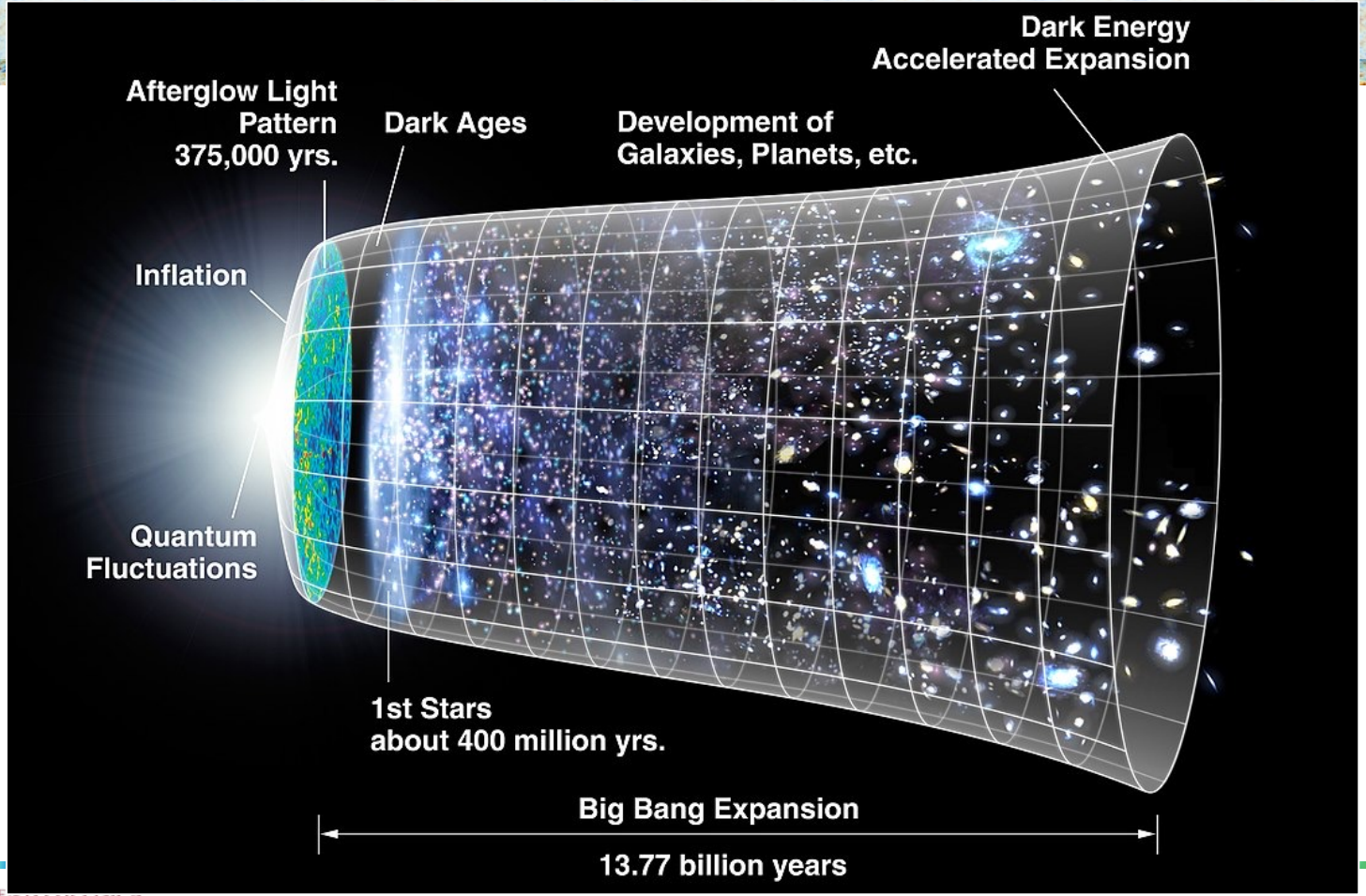
Dark Energy
Accelerated Expansion
Afterglow Light
Pattern
375,000 yrs.
Dark Ages
Development of
Galaxies, Planets, etc.
Inflation
Quantum
Fluctuations
1st Stars
about 400 million yrs.
Big Bang Expansion
13.77 billion years

CMB observations - target signals

Target signal 1: CMB anisotropy at small angular scales, to improve cosmological parameters determination

Target signal 2: CMB E-mode polarization at large scales, probes the Universe re-ionization (first stars)

Target signal 3: Lensing effects due to distribution of large-scale structures (dark matter)

Target signal 4 (B-modes): Inflationary gravitational waves
Not measured by other probes
Signal unknown - **parameter *r***
To probe inflationary physics at extremely high energy

Target signal 5: spectral distortions, to probe physical processes just before the CMB image formation, dark-matter annihilation, and more

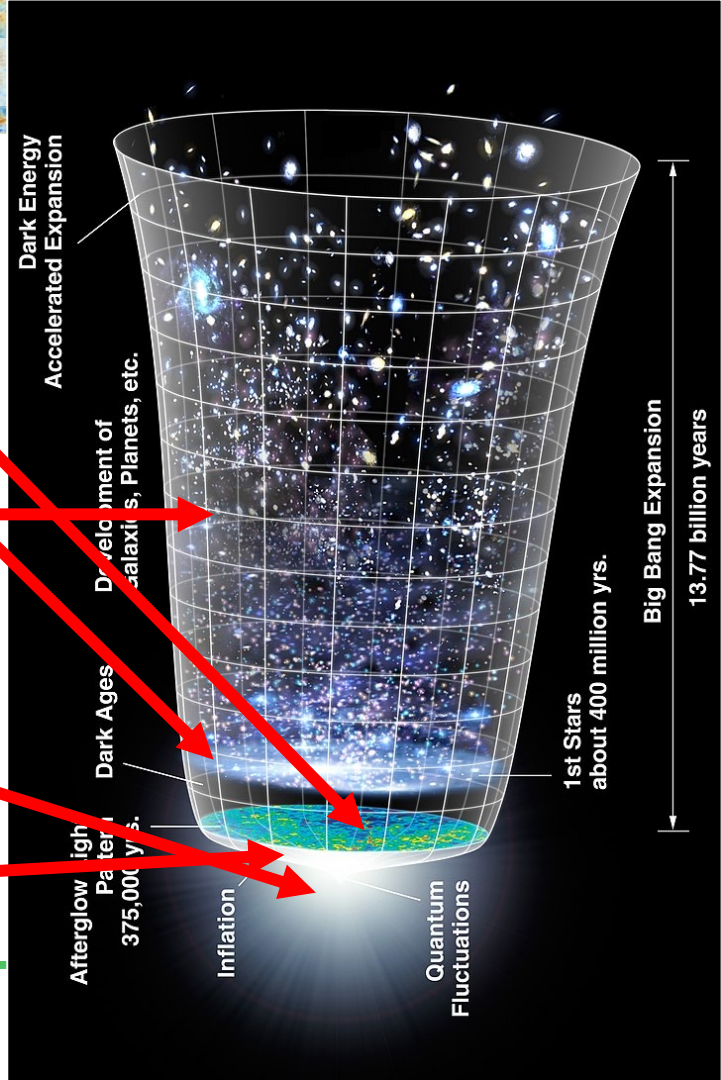

CMB observations - target signals

Target signal 1: CMB anisotropy at small angular scales, to improve cosmological parameters determination

Target signal 2: CMB E-mode polarization at large scales, probes the Universe re-ionization (first stars)

Target signal 3: Lensing effects due to distribution of large-scale structures (dark matter)

Target signal 4 (B-modes): Inflationary gravitational waves
Not measured by other probes
Signal unknown - **parameter *r***
To probe inflationary physics at extremely high energy

Target signal 5: spectral distortions, to probe physical processes just before the CMB image formation, dark-matter annihilation, and more

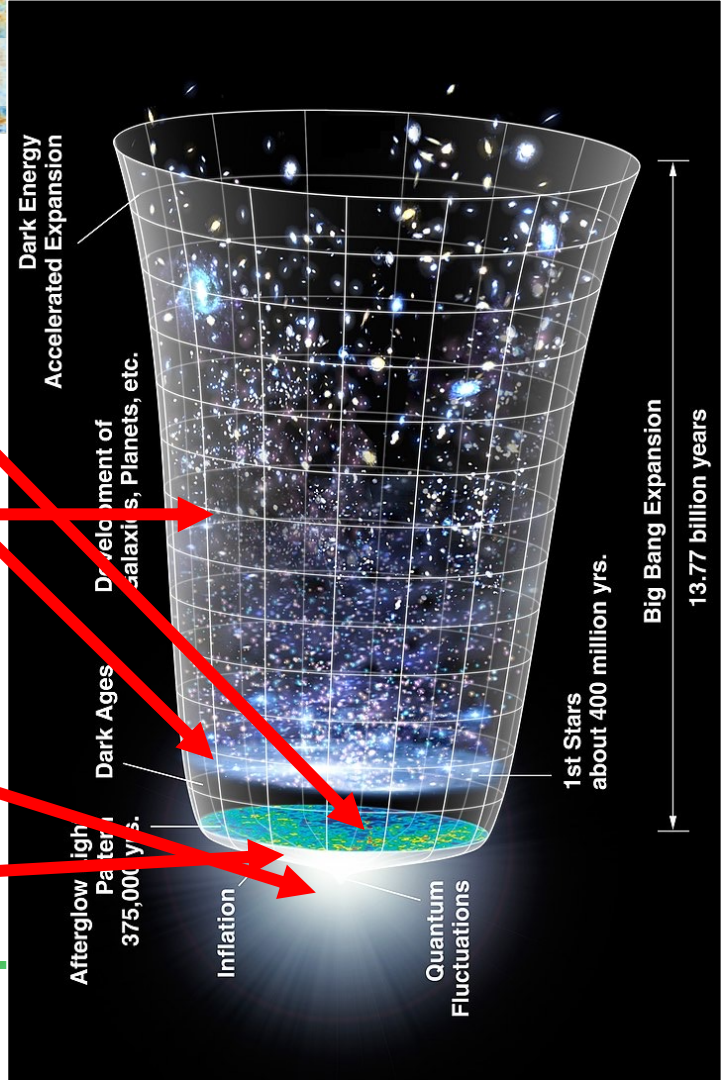

Measured quantity (CMB temperature anisotropy, to start with)

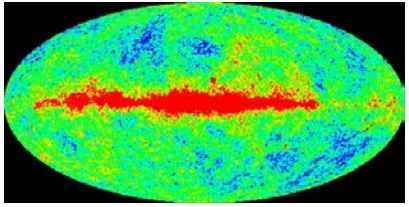

$$BB(\nu,T) = \frac{2h\nu^3}{c^2}\frac{1}{e^{\frac{h\nu}{kT}}-1} \qquad x = \frac{h\nu}{KT}$$

Blackbody radiation

$$\Delta B(\nu,T) = \left.\frac{dBB(\nu,T)}{dT}\right|_{T=T_{cmb}} \Delta T$$

Brightness variation [W/m^2/sr/Hz] for Temperature variation

$$\Delta B(\nu,T) = \frac{xe^x}{e^x-1}\frac{BB(\nu,T_{cmb})}{T_{cmb}}\Delta T$$

$$\Delta P = \Delta T \int_0^\infty A\Omega\eta f(\nu)\frac{xe^x}{e^x-1}\frac{BB(\nu,T_{cmb})}{T_{cmb}}d\nu$$

Power variation on the detector

$$\Delta T[\mathrm{K_{cmb}}] = \frac{\Delta P[\mathrm{W}]}{\int_0^\infty A\Omega\eta f(\nu)\frac{xe^x}{e^x-1}\frac{BB(\nu,T_{cmb})}{T_{cmb}}d\nu}$$

expressed in terms of temperature fluctuation

Angular power spectrum

$$\Delta T(\hat{n}) = \sum_{l=0}^{\infty} \sum_{m=-l}^{l} a_{lm} Y_{lm}(\hat{n})$$

Spherical harmonics decomposition

$$a_{lm} = \int_{4\pi} Y^*_{lm}(\hat{n}) \Delta T(\hat{n}) d\Omega$$

coefficients

$$\langle a^*_{l'm'} a_{lm} \rangle_{\text{ensemble}}$$

if the statistics is Gaussian, the information is encoded in the variance of the coefficients

$$\langle a^*_{l'm'} a_{lm} \rangle_{\text{ens}} = C_\ell \delta_{ll'} \delta_{mm'}$$

assuming “isotropy” (no preferred directions) and linearity this depends only on ell, and there is no cross-correlation among different multipole numbers

Angular power spectrum

Instead of the CMB map, its angular power spectrum is used to measure the statistical properties.

These statistical properties are related to the properties of the Universe, encoded in the cosmological parameters

The angular power spectrum is the basic instrument to compare data and models

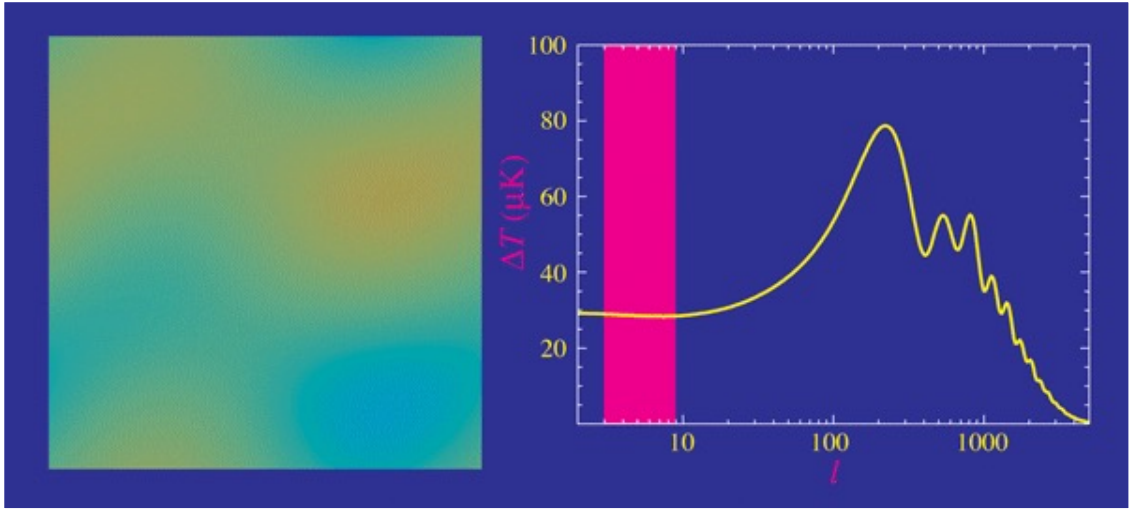

Credit http://background.uchicago.edu/~whu/metaanim.html

Angular power spectrum estimator

$$\langle a^*_{l'm'} a_{lm} \rangle_{\rm ens} = C_\ell \delta_{ll'} \delta_{mm'}$$

$$\hat{C}_l = \frac{1}{2l+1} \sum_{m=-l}^{l} a^*_{lm} a_{lm}$$

$$\begin{aligned} \langle \hat{C}_l \rangle_{\rm ens} &= \frac{1}{2l+1} \sum_{m=-l}^{l} \langle a^*_{lm} a_{lm} \rangle_{\rm ens} \\ &= \frac{2l+1}{2l+1} \langle a^*_{lm} a_{lm} \rangle_{\rm ens} \\ &= C_l \end{aligned}$$

We don't have an ensemble of universes to average on !

Error on $\hat{C}_l$

Compute the sampling variance of the estimator

$$\mathrm{Var}(\hat{C}_l) = \left\langle \left(\hat{C}_l - \langle \hat{C}_l \rangle\right)^2 \right\rangle_{ms}$$

$$= \left\langle \hat{C}_l^2 + \langle \hat{C}_l \rangle^2 - 2\hat{C}_l \langle \hat{C}_l \rangle \right\rangle$$

$$= \langle \hat{C}_l^2 \rangle + \langle \hat{C}_l \rangle^2 - 2\langle \hat{C}_l \rangle^2$$

$$= \langle \hat{C}_l^2 \rangle - \langle \hat{C}_l \rangle^2$$

$$= \left(\frac{1}{2l+1}\sum_m a_{lm} a_{lm}^*\right)\left(\frac{1}{2l+1}\sum_{m'} a_{lm'} a_{lm'}^*\right) - C_l^2$$

$$= \frac{1}{(2l+1)^2}\left(\sum_m \langle a_{lm} a_{lm}^* a_{lm} a_{lm}^* \rangle + \sum_m \sum_{m' \neq m} \langle a_{lm} a_{lm}^* a_{lm'} a_{lm'}^* \rangle\right) - C_l^2$$

$2l+1$ terms

$(2l+1)\,2l$ terms

$$= \frac{1}{(2l+1)^2}\left((2l+1)\, 3\, C_l^2 + (2l+1)\, 2l\, C_l^2\right) - C_l^2$$

(four moment of a gaussian distribution $\langle x^4 \rangle = 3(\sigma^2)^2$)

$$= \frac{1}{(2l+1)^2}\left[3(2l+1) + 2l(2l+1) - (2l+1)^2\right] C_l^2$$

$$= \frac{1}{2l+1}\left(3 + 2l - 2l - 1\right) C_l^2 = \frac{2}{2l+1} C_l^2$$

Cosmic variance

$$\Delta\hat{C}_l = \sqrt{\frac{2}{2l+1}} C_l \simeq \sqrt{\frac{2}{2l+1}} \hat{C}_l$$

Angular response effect

Given a limited angular resolution, the measured spherical harmonic coefficients are not the sky a_{lm}

$$d_{lm} = \int_{4\pi} d\Omega \int_{4\pi} d\Omega' B(\theta' - \theta, \phi' - \phi) \Delta T(\theta', \phi') Y^*_{lm} = a_{lm} b_{lm}$$

(the convolution is a product in reciprocal space)

b_l are the spherical harmonic coefficients of the angular response

In the simplest case

$$b_{lm} = B_l = \exp\left(-0.5\ l\ (l+1)\ \sigma^2_{\rm beam}\right)$$

For the power spectrum

$$\hat{C}_l^{\rm obs} = B_l^2 \hat{C}_l$$

Error in the power spectrum in the case of a map with signal and noise

In presence of signal (beam smoothed) and noise

$$d_{lm} = B_l a_{lm} + n_{lm}$$

$$\langle d^*_{lm} d_{lm} \rangle = B^2_{lm} \langle a^*_{lm} a_{lm} \rangle + B^*_{lm} \langle a^*_{lm} n_{lm} \rangle + B_{lm} \langle n^*_{lm} a_{lm} \rangle + \langle n^*_{lm} n_{lm} \rangle$$

$$\hat{D}_l = B_l^2 \hat{C}_l + N_l$$

N_l is the "noise bias" to be estimated and removed

$$\tilde{C}_l = \frac{\hat{D}_l - \tilde{N}_l}{B_l^2}$$

New estimator

$\tilde{N}_l$ is an estimation of the noise bias (see next slides)

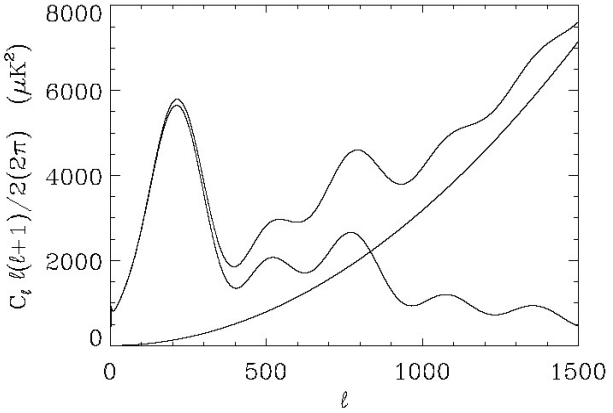

$$\mathrm{Var}(\tilde{C}_l) = \frac{\mathrm{Var}(\hat{D}_l)}{B_l^2} = \frac{2}{2l+1}\left(\hat{C}_l + \frac{N_l}{B_l^2}\right)^2$$

$$\Delta\tilde{C}_l = \sqrt{\frac{2}{2l+1}}\left(\hat{C}_l + \frac{N_l}{B_l^2}\right)$$

Noise bias estimation

The **photon noise** is the ineliminable noise term due to randomness of photons arriving on the detector

Given a signal with brightness I_ν [$Wm^{-2}sz^{-1}Hz^{-1}$], the power hitting the detector is $P = \int f_\nu \eta A \Omega I_\nu d\nu$

f_ν is the filter, η is the efficiency (including 50% for polarization)

and the photon noise can be computed as $$\mathrm{NEP}^2_{\mathrm{ph}} = 2 \int f_\nu \eta A \Omega I_\nu h\nu \left(1 + \frac{f_\nu \eta c^2 I_\nu}{h\nu^3}\right) d\nu.$$

To this term, is to be added the **thermal noise** in the detector $\mathrm{NEP}^2_{\mathrm{thermal}} = 4 k_B G T^2$

The **readout noise** depends on the detector technology, and is such that $NEP^2_{readout} << NEP^2_{ph}$

The total noise is added in quadrature, and converted back to CMB temperature fluctuation

$$\mathrm{NET}_{\mathrm{tot}}[\mathrm{K_{cmb}Hz^{-1/2}}] = \frac{\mathrm{NEP}_{\mathrm{tot}}}{\int_0^\infty A\Omega\eta f(\nu) \frac{xe^x}{e^x-1} \frac{BB_\nu(T_{cmb})}{T_{cmb}} d\nu}$$

$$\mathrm{NET}_{\mathrm{tot}}[\mathrm{K_{cmb}s^{1/2}}] = \frac{\mathrm{NEP}_{\mathrm{tot}}}{\int_0^\infty A\Omega\eta f(\nu) \frac{xe^x}{e^x-1} \frac{BB_\nu(T_{cmb})}{T_{cmb}} d\nu} \frac{1}{\sqrt{2}}$$

From detector noise to map noise

$$\sigma^2_{pix} = NET^2 \frac{1}{NT_{pix}}$$

$$T_{pix} = \frac{T}{N_{pix}}$$

$$N_{pix} = \frac{4\pi f}{\Omega_{pix}}$$

$$T_{pix} = \frac{T\Omega_{pix}}{4\pi f}$$

$$\sigma^2_{pix} = NET^2 \frac{4\pi f}{TN\Omega_{pix}}$$

In terms of angular power spectrum, we can remember that the 2-points correlation function is the Legendre transform of the angular power spectrum

$$c(\theta) = \langle \Delta T(\hat{n}) \Delta T(\hat{n}') \rangle; \quad \text{where } \hat{n} \cdot \hat{n}' = \cos\theta$$

$$c(\theta) = \frac{1}{4\pi} \sum_{\ell=0}^{\infty} (2\ell+1) C_\ell P_\ell(\cos\theta)$$

$$\sigma^2_{pix} = c(\theta = 0) = \frac{1}{4\pi} \sum_{l=0}^{\infty} (2l+1) C_l$$

From map noise to power spectrum of the noise

Compute angular power spectrum of a white noise map N_l = *const*

Noise only map

Sky divided in *n* pixels

The standard deviation in a pixel (previous slide) is, in case of full sky observation

$$\sigma^2_{pix} = C(\theta = 0) = \frac{1}{4\pi}\sum N_\ell(2\ell+1) = \frac{N_\ell}{4\pi}\sum(2\ell+1)$$

We don't have an infinite number of multipole to sum over. The number of data in the map is N_{pix}, and must be the same in pixel space and in harmonic space, then

$$\sum_{l=0}^{l_{max}}\sum_{m=-l}^{l} 1 = \sum_{l=0}^{l_{max}}(2l+1) = N_{pix}$$

Then

$$\sigma^2_{pix} = \frac{N_\ell}{4\pi}N_{pix}$$

$$N_l = \frac{4\pi}{N_{pix}}\sigma^2_{pix} = \Omega_{pix}\sigma^2_{pix}$$

This is the power spectrum of the noise, not the error of the power spectrum

$$N_l = \frac{4\pi \mathrm{NET}^2}{TN}$$

The observed sky fraction *f* is cancelled (N_l is valid for full sky)

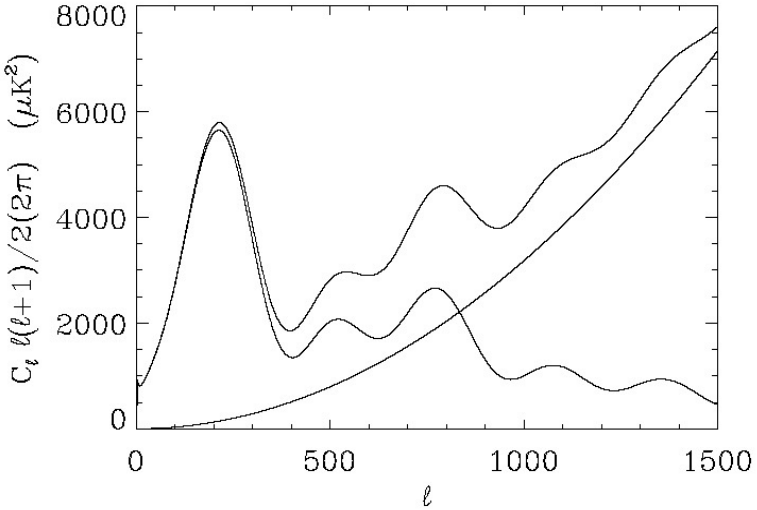

$$\tilde{C}_l = \frac{\hat{D}_l - \tilde{N}_l}{B_l^2}$$

$$\Delta\tilde{C}_l = \sqrt{\frac{2}{2l+1}}\left(\hat{C}_l + \frac{N_l}{B_l^2}\right)$$

$$N_l = \frac{4\pi \mathrm{NET}^2}{TN}$$

$$\Delta\tilde{C}_l = \sqrt{\frac{2}{2l+1}}\left(\hat{C}_l + \frac{4\pi \mathrm{NET}^2}{TNB_l^2}\right)$$

In case of a sky fraction *f* observed

$$\Delta\tilde{C}_l = \sqrt{\frac{2}{(2l+1)f}}\left(\hat{C}_l + \frac{4\pi \mathrm{NET}^2}{TNB_l^2}\right)$$

The CMB polarization

Simple Thomson scattering of em wave off electrons can polarize it

$$\frac{d\sigma}{d\Omega} = \frac{3\sigma_T}{8\pi}|\hat{\epsilon}\cdot\hat{\epsilon}'|^2$$

differential cross-section with ϵ and ϵ' input and output polarization

90 deg scattering => fully polarized radiation

If the incoming radiation has uniform or dipole distribution

=> no polarization

If the incoming radiation has a quadrupolar distribution

=> polarization

We need to identify possible sources of quadrupolar distribution of radiation

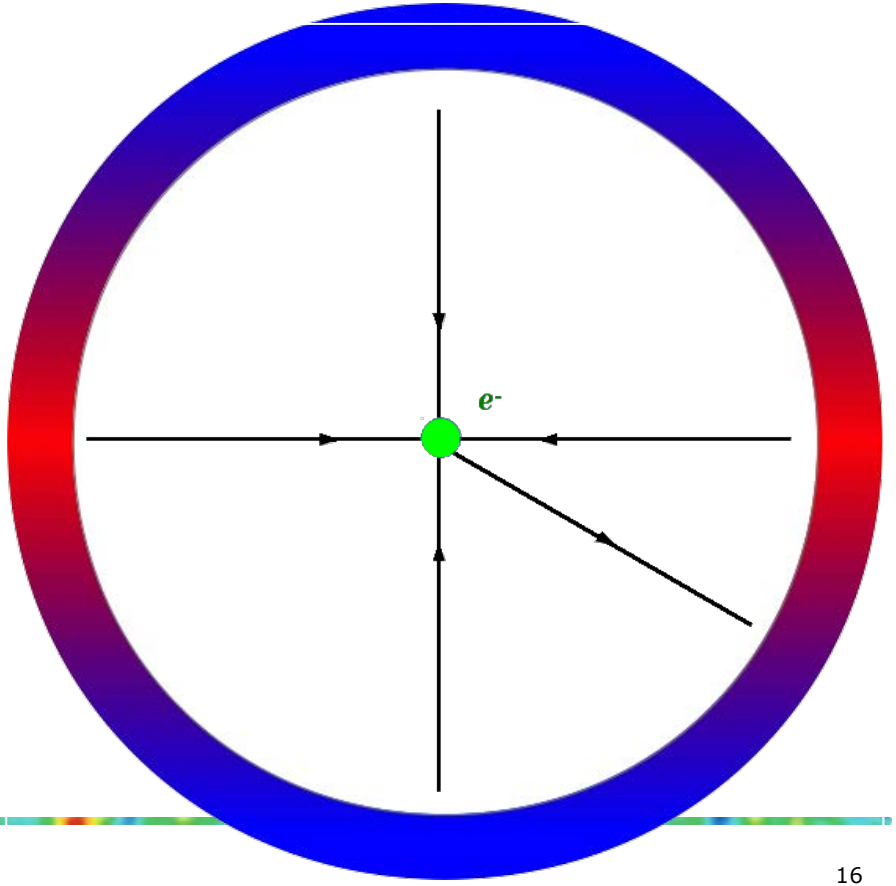

Polarized signal

In case of linear polarization (*I*, *Q*, *U*) Stokes parameters and a detector sensitive to one polarization only

The Stokes parameters of the CMB are function of the direction in the sky, $\hat{n}$, and two directions perpendicular to $\hat{n}$ that are used to define Q and U, ($\hat{\mathbf{e}}_1$, $\hat{\mathbf{e}}_2$), that correspond to spherical coordinate system ($\hat{\mathbf{e}}_\theta$, $\hat{\mathbf{e}}_\phi$). While the intensity I is invariant under rotation in the ($\hat{\mathbf{e}}_1$, $\hat{\mathbf{e}}_2$) plane, Q and U transform under a rotation of an angle ψ as

$$\begin{aligned}(Q+iU)'(\hat{n}) &= e^{-2i\psi}(Q+iU)(\hat{n}) \\ (Q-iU)'(\hat{n}) &= e^{+2i\psi}(Q-iU)(\hat{n})\end{aligned} \tag{1.80}$$

The quantities $Q \pm iU$ are named spin-2. The statistical properties of the radiation field are usually described in terms the spherical harmonic decomposition of the maps. This basis is very natural because the statistical properties of anisotropy are rotationally invariant. The standard spherical harmonics are not the appropriate basis for $Q \pm iU$ because they are spin-2 variables, but a generalization exists, the spin weighted basis [112], ${}_{\pm 2}Y_{lm}$, that is used to expand $Q \pm iU$ as

$$\begin{aligned}(Q+iU)(\hat{n}) &= \textstyle\sum_{l,m} a_{+2,lm}\ {}_{+2}Y_{lm}(\hat{n}) \\ (Q-iU)(\hat{n}) &= \textstyle\sum_{l,m} a_{-2,lm}\ {}_{-2}Y_{lm}(\hat{n})\end{aligned} \tag{1.81}$$

where the relation $a^*_{-2,lm} = a_{2,l-m}$ must be satisfied.

Instead of $a_{\pm 2,lm}$ it is convenient to introduce their linear combination

$$\begin{aligned}a_{E,lm} &= -\tfrac{1}{2}(a_{2,lm} + a_{-2,lm}) \\ a_{B,lm} &= \tfrac{1}{2}i(a_{2,lm} - a_{-2,lm})\end{aligned} \tag{1.82}$$

$$E(\boldsymbol{n}) = \sum_{lm} \sqrt{\frac{(l+2)!}{(l-2)!}}\, a_{E,lm}\, Y_{lm}(\boldsymbol{n}),$$

$$B(\boldsymbol{n}) = \sum_{lm} \sqrt{\frac{(l+2)!}{(l-2)!}}\, a_{B,lm}\, Y_{lm}(\boldsymbol{n}),$$

$$C_{Tl} = \frac{1}{2l+1}\sum_m \langle a^*_{T,lm} a_{T,lm}\rangle, \qquad \langle a^*_{T,l'm'} a_{T,lm}\rangle = C_{Tl}\delta_{l'l}\delta_{m'm},$$

$$C_{El} = \frac{1}{2l+1}\sum_m \langle a^*_{E,lm} a_{E,lm}\rangle, \qquad \langle a^*_{E,l'm'} a_{E,lm}\rangle = C_{El}\delta_{l'l}\delta_{m'm},$$

$$C_{Bl} = \frac{1}{2l+1}\sum_m \langle a^*_{B,lm} a_{B,lm}\rangle, \qquad \langle a^*_{B,l'm'} a_{B,lm}\rangle = C_{Bl}\delta_{l'l}\delta_{m'm},$$

$$\langle a^*_{T,l'm'} a_{E,lm}\rangle = C_{Cl}\delta_{l'l}\delta_{m'm},$$

$$C_{Cl} = \frac{1}{2l+1}\sum_m \langle a^*_{T,lm} a_{E,lm}\rangle, \qquad \langle a^*_{B,l'm'} a_{E,lm}\rangle = \langle a^*_{B,l'm'} a_{T,lm}\rangle = 0.$$

The sensitivity for intensity signal is

$$\Delta\tilde{C}_l = \sqrt{\frac{2}{(2l+1)f}}\left(\hat{C}_l + \frac{4\pi \mathrm{NET}^2}{TNB_l^2}\right)$$

For polarized signal

$$\Delta\tilde{C}_l = \sqrt{\frac{2}{(2l+1)f}}\left(\hat{C}_l + \frac{4\pi\ 2\,\mathrm{NET}^2}{TNB_l^2}\right)$$

Planck temperature anisotropy angular power spectrum

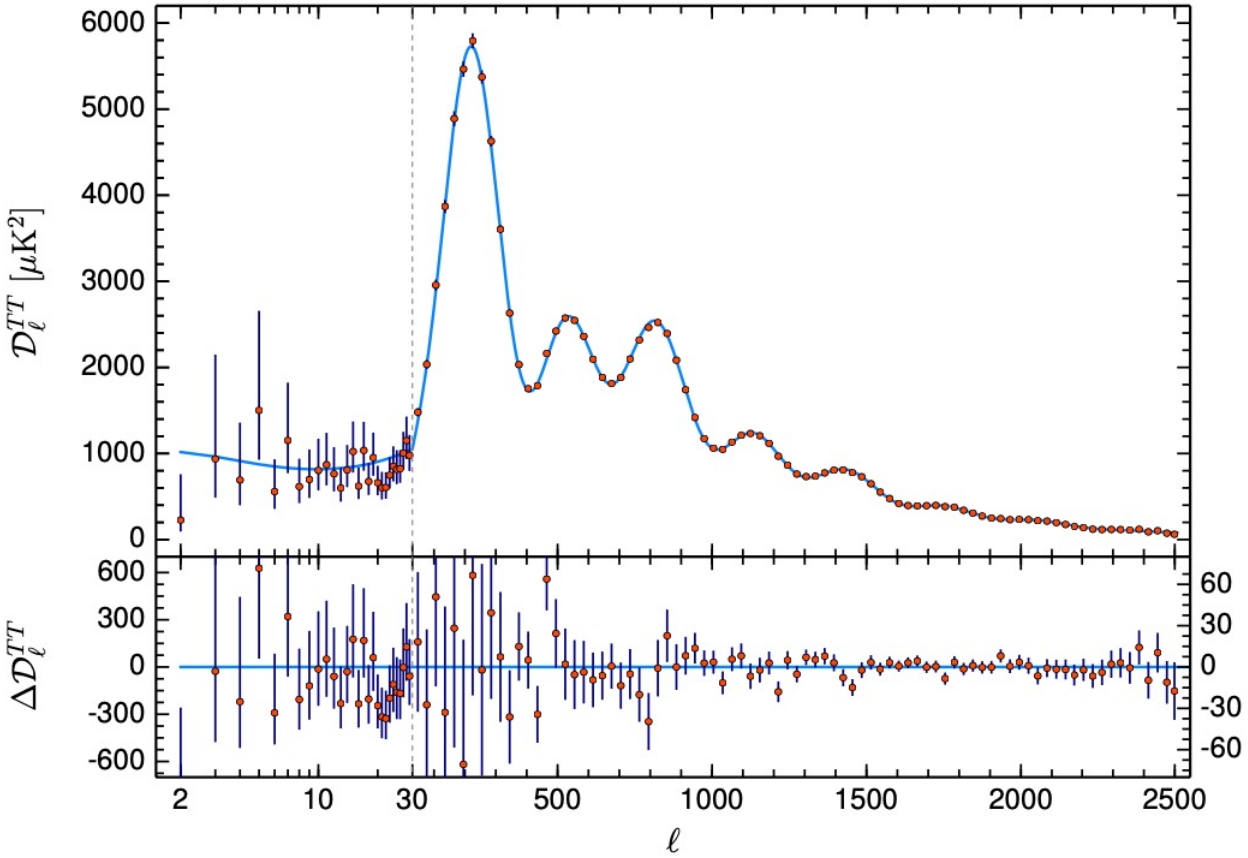

Planck results

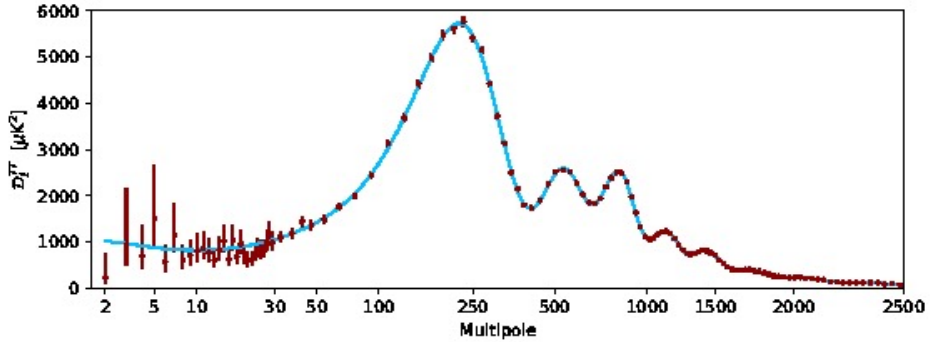

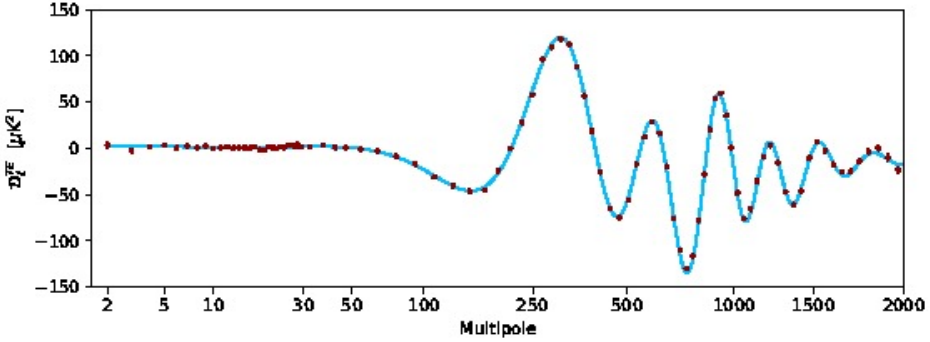

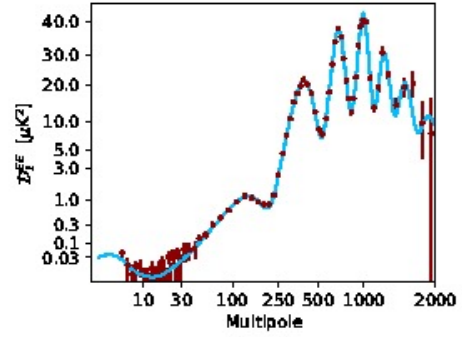

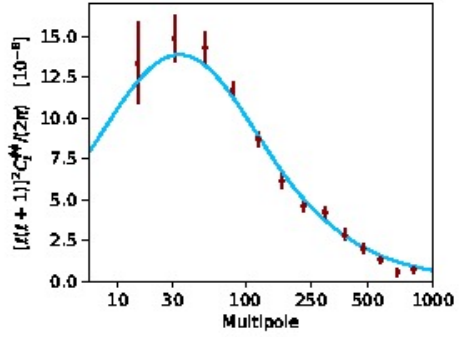

Λ-CDM model

Planck 2013 results. XVI. Cosmological parameters

Table 1. Cosmological parameters used in our analysis. For each, we give the symbol, prior range, value taken in the base ΛCDM cosmology (where appropriate), and summary definition (see text for details). The top block contains parameters with uniform priors that are varied in the MCMC chains. The ranges of these priors are listed in square brackets. The lower blocks define various derived parameters.

Parameter	Prior range	Baseline	Definition
$\omega_b \equiv \Omega_b h^2$	$[0.005, 0.1]$	...	Baryon density today
$\omega_c \equiv \Omega_c h^2$	$[0.001, 0.99]$	...	Cold dark matter density today
$100\theta_{MC}$	$[0.5, 10.0]$	...	$100\times$ approximation to r_*/D_A (CosmoMC)
τ	$[0.01, 0.8]$	...	Thomson scattering optical depth due to reionization
Ω_K	$[-0.3, 0.3]$	0	Curvature parameter today with $\Omega_{tot} = 1 - \Omega_K$
$\sum m_\nu$	$[0, 5]$	0.06	The sum of neutrino masses in eV
$m^{eff}_{\nu,\,sterile}$	$[0, 3]$	0	Effective mass of sterile neutrino in eV
w_0	$[-3.0, -0.3]$	-1	Dark energy equation of state[a], $w(a) = w_0 + (1-a)w_a$
w_a	$[-2, 2]$	0	As above (perturbations modelled using PPF)
N_{eff}	$[0.05, 10.0]$	3.046	Effective number of neutrino-like relativistic degrees of freedom (see text)
Y_P	$[0.1, 0.5]$	BBN	Fraction of baryonic mass in helium
A_L	$[0, 10]$	1	Amplitude of the lensing power relative to the physical value
n_s	$[0.9, 1.1]$	...	Scalar spectrum power-law index ($k_0 = 0.05\mathrm{Mpc}^{-1}$)
n_t	$n_t = -r_{0.05}/8$	Inflation	Tensor spectrum power-law index ($k_0 = 0.05\mathrm{Mpc}^{-1}$)
$dn_s/d\ln k$	$[-1, 1]$	0	Running of the spectral index
$\ln(10^{10}A_s)$	$[2.7, 4.0]$	...	Log power of the primordial curvature perturbations ($k_0 = 0.05\,\mathrm{Mpc}^{-1}$)
$r_{0.05}$	$[0, 2]$	0	Ratio of tensor primordial power to curvature power at $k_0 = 0.05\,\mathrm{Mpc}^{-1}$
Ω_Λ		...	Dark energy density divided by the critical density today
t_0		...	Age of the Universe today (in Gyr)
Ω_m		...	Matter density (inc. massive neutrinos) today divided by the critical density
σ_8		...	RMS matter fluctuations today in linear theory
z_{re}		...	Redshift at which Universe is half reionized
H_0	$[20, 100]$	...	Current expansion rate in $\mathrm{km\,s^{-1}Mpc^{-1}}$
$r_{0.002}$		0	Ratio of tensor primordial power to curvature power at $k_0 = 0.002\,\mathrm{Mpc}^{-1}$
$10^9 A_s$		...	$10^9\times$ dimensionless curvature power spectrum at $k_0 = 0.05\,\mathrm{Mpc}^{-1}$
$\omega_m \equiv \Omega_m h^2$		...	Total matter density today (inc. massive neutrinos)
z_*		...	Redshift for which the optical depth equals unity (see text)
$r_* = r_s(z_*)$		...	Comoving size of the sound horizon at $z = z_*$
$100\theta_*$		...	$100\times$ angular size of sound horizon at $z = z_*$ (r_*/D_A)
z_{drag}		...	Redshift at which baryon-drag optical depth equals unity (see text)
$r_{drag} = r_s(z_{drag})$		...	Comoving size of the sound horizon at $z = z_{drag}$
k_D		...	Characteristic damping comoving wavenumber (Mpc^{-1})
$100\theta_D$		...	$100\times$ angular extent of photon diffusion at last scattering (see text)
z_{eq}		...	Redshift of matter-radiation equality (massless neutrinos)
$100\theta_{eq}$		...	$100\times$ angular size of the comoving horizon at matter-radiation equality
$r_{drag}/D_V(0.57)$		...	BAO distance ratio at $z = 0.57$ (see Sect. 5.2)

[a] For dynamical dark energy models with constant equation of state, we denote the equation of state by w and adopt the same prior as for w_0.

Λ-CDM model

Planck 2013 results. XVI. Cosmological parameters

Table 1. Cosmological parameters used in our analysis. For each, we give the symbol, prior range, value taken in the base ΛCDM cosmology (where appropriate), and summary definition (see text for details). The top block contains parameters with uniform priors that are varied in the MCMC chains. The ranges of these priors are listed in square brackets. The lower blocks define various derived parameters.

Parameter	Prior range	Baseline	Definition
$\omega_b \equiv \Omega_b h^2$	$[0.005, 0.1]$	...	Baryon density today
$\omega_c \equiv \Omega_c h^2$	$[0.001, 0.99]$	...	Cold dark matter density today
$100\theta_{MC}$	$[0.5, 10.0]$	...	$100\times$ approximation to r_*/D_A (CosmoMC)
τ	$[0.01, 0.8]$	...	Thomson scattering optical depth due to reionization
Ω_K	$[-0.3, 0.3]$	0	Curvature parameter today with $\Omega_{tot} = 1 - \Omega_K$
$\sum m_\nu$	$[0, 5]$	0.06	The sum of neutrino masses in eV
$m^{eff}_{\nu,\,sterile}$	$[0, 3]$	0	Effective mass of sterile neutrino in eV
w_0	$[-3.0, -0.3]$	-1	Dark energy equation of state[a], $w(a) = w_0 + (1-a)w_a$
w_a	$[-2, 2]$	0	As above (perturbations modelled using PPF)
N_{eff}	$[0.05, 10.0]$	3.046	Effective number of neutrino-like relativistic degrees of freedom (see text)
Y_P	$[0.1, 0.5]$	BBN	Fraction of baryonic mass in helium
A_L	$[0, 10]$	1	Amplitude of the lensing power relative to the physical value
n_s	$[0.9, 1.1]$	...	Scalar spectrum power-law index ($k_0 = 0.05\mathrm{Mpc}^{-1}$)
n_t	$n_t = -r_{0.05}/8$	Inflation	Tensor spectrum power-law index ($k_0 = 0.05\mathrm{Mpc}^{-1}$)
$dn_s/d\ln k$	$[-1, 1]$	0	Running of the spectral index
$\ln(10^{10}A_s)$	$[2.7, 4.0]$	...	Log power of the primordial curvature perturbations ($k_0 = 0.05\,\mathrm{Mpc}^{-1}$)
$r_{0.05}$	$[0, 2]$	0	Ratio of tensor primordial power to curvature power at $k_0 = 0.05\,\mathrm{Mpc}^{-1}$
Ω_Λ		...	Dark energy density divided by the critical density today
t_0		...	Age of the Universe today (in Gyr)
Ω_m		...	Matter density (inc. massive neutrinos) today divided by the critical density
σ_8		...	RMS matter fluctuations today in linear theory
z_{re}		...	Redshift at which Universe is half reionized
H_0	$[20, 100]$	...	Current expansion rate in $\mathrm{km\,s^{-1}Mpc^{-1}}$
$r_{0.002}$		0	Ratio of tensor primordial power to curvature power at $k_0 = 0.002\,\mathrm{Mpc}^{-1}$
$10^9 A_s$		...	$10^9\times$ dimensionless curvature power spectrum at $k_0 = 0.05\,\mathrm{Mpc}^{-1}$
$\omega_m \equiv \Omega_m h^2$		...	Total matter density today (inc. massive neutrinos)
z_*		...	Redshift for which the optical depth equals unity (see text)
$r_* = r_s(z_*)$		...	Comoving size of the sound horizon at $z = z_*$
$100\theta_*$		...	$100\times$ angular size of sound horizon at $z = z_*$ (r_*/D_A)
z_{drag}		...	Redshift at which baryon-drag optical depth equals unity (see text)
$r_{drag} = r_s(z_{drag})$		...	Comoving size of the sound horizon at $z = z_{drag}$
k_D		...	Characteristic damping comoving wavenumber (Mpc^{-1})
$100\theta_D$		...	$100\times$ angular extent of photon diffusion at last scattering (see text)
z_{eq}		...	Redshift of matter-radiation equality (massless neutrinos)
$100\theta_{eq}$		...	$100\times$ angular size of the comoving horizon at matter-radiation equality
$r_{drag}/D_V(0.57)$		...	BAO distance ratio at $z = 0.57$ (see Sect. 5.2)

[a] For dynamical dark energy models with constant equation of state, we denote the equation of state by w and adopt the same prior as for w_0.

Λ-CDM 6 parameters model

Planck 2018 results. VI. Cosmological parameters

	Parameter	Plik best fit	Plik [1]	CamSpec [2]	$([2]-[1])/\sigma_1$	Combined
Baryon density	$\Omega_b h^2$	0.022383	0.02237 ± 0.00015	0.02229 ± 0.00015	−0.5	0.02233 ± 0.00015
Cold Dark Matter density	$\Omega_c h^2$	0.12011	0.1200 ± 0.0012	0.1197 ± 0.0012	−0.3	0.1198 ± 0.0012
Angular scale of CMB peaks	$100\theta_{MC}$	1.040909	1.04092 ± 0.00031	1.04087 ± 0.00031	−0.2	1.04089 ± 0.00031
Optical depth of the universe	τ	0.0543	0.0544 ± 0.0073	$0.0536^{+0.0069}_{-0.0077}$	−0.1	0.0540 ± 0.0074
Primordial perturbations amplitude	$\ln(10^{10} A_s)$	3.0448	3.044 ± 0.014	3.041 ± 0.015	−0.3	3.043 ± 0.014
Primordial perturbation spectral index	n_s	0.96605	0.9649 ± 0.0042	0.9656 ± 0.0042	+0.2	0.9652 ± 0.0042
Matter density	$\Omega_m h^2$	0.14314	0.1430 ± 0.0011	0.1426 ± 0.0011	−0.3	0.1428 ± 0.0011
Hubble constant	H_0 [km s^{-1}Mpc^{-1}]	67.32	67.36 ± 0.54	67.39 ± 0.54	+0.1	67.37 ± 0.54
Matter density	Ω_m	0.3158	0.3153 ± 0.0073	0.3142 ± 0.0074	−0.2	0.3147 ± 0.0074
Age of the Universe	Age [Gyr]	13.7971	13.797 ± 0.023	13.805 ± 0.023	+0.4	13.801 ± 0.024
LSS fluctuation amplitude today	σ_8	0.8120	0.8111 ± 0.0060	0.8091 ± 0.0060	−0.3	0.8101 ± 0.0061
	$S_8 \equiv \sigma_8(\Omega_m/0.3)^{0.5}$	0.8331	0.832 ± 0.013	0.828 ± 0.013	−0.3	0.830 ± 0.013
Recombination redshift	z_{re}	7.68	7.67 ± 0.73	7.61 ± 0.75	−0.1	7.64 ± 0.74
	$100\theta_*$	1.041085	1.04110 ± 0.00031	1.04106 ± 0.00031	−0.1	1.04108 ± 0.00031
	r_{drag} [Mpc]	147.049	147.09 ± 0.26	147.26 ± 0.28	+0.6	147.18 ± 0.29

Λ-CDM model

Planck 2013 results. XVI. Cosmological parameters

Table 1. Cosmological parameters used in our analysis. For each, we give the symbol, prior range, value taken in the base ΛCDM cosmology (where appropriate), and summary definition (see text for details). The top block contains parameters with uniform priors that are varied in the MCMC chains. The ranges of these priors are listed in square brackets. The lower blocks define various derived parameters.

Parameter	Prior range	Baseline	Definition
$\omega_b \equiv \Omega_b h^2$	$[0.005, 0.1]$	...	Baryon density today
$\omega_c \equiv \Omega_c h^2$	$[0.001, 0.99]$	...	Cold dark matter density today
$100\theta_{MC}$	$[0.5, 10.0]$	...	$100\times$ approximation to r_*/D_A (CosmoMC)
τ	$[0.01, 0.8]$	...	Thomson scattering optical depth due to reionization
Ω_K	$[-0.3, 0.3]$	0	Curvature parameter today with $\Omega_{tot} = 1 - \Omega_K$
$\sum m_\nu$	$[0, 5]$	0.06	The sum of neutrino masses in eV
$m^{eff}_{\nu,\,sterile}$	$[0, 3]$	0	Effective mass of sterile neutrino in eV
w_0	$[-3.0, -0.3]$	-1	Dark energy equation of state[a], $w(a) = w_0 + (1-a)w_a$
w_a	$[-2, 2]$	0	As above (perturbations modelled using PPF)
N_{eff}	$[0.05, 10.0]$	3.046	Effective number of neutrino-like relativistic degrees of freedom (see text)
Y_P	$[0.1, 0.5]$	BBN	Fraction of baryonic mass in helium
A_L	$[0, 10]$	1	Amplitude of the lensing power relative to the physical value
n_s	$[0.9, 1.1]$	...	Scalar spectrum power-law index ($k_0 = 0.05\mathrm{Mpc}^{-1}$)
n_t	$n_t = -r_{0.05}/8$	Inflation	Tensor spectrum power-law index ($k_0 = 0.05\mathrm{Mpc}^{-1}$)
$dn_s/d\ln k$	$[-1, 1]$	0	Running of the spectral index
$\ln(10^{10}A_s)$	$[2.7, 4.0]$	...	Log power of the primordial curvature perturbations ($k_0 = 0.05\,\mathrm{Mpc}^{-1}$)
$r_{0.05}$	$[0, 2]$	0	Ratio of tensor primordial power to curvature power at $k_0 = 0.05\,\mathrm{Mpc}^{-1}$
Ω_Λ		...	Dark energy density divided by the critical density today
t_0		...	Age of the Universe today (in Gyr)
Ω_m		...	Matter density (inc. massive neutrinos) today divided by the critical density
σ_8		...	RMS matter fluctuations today in linear theory
z_{re}		...	Redshift at which Universe is half reionized
H_0	$[20, 100]$	...	Current expansion rate in $\mathrm{km\,s^{-1}Mpc^{-1}}$
$r_{0.002}$		0	Ratio of tensor primordial power to curvature power at $k_0 = 0.002\,\mathrm{Mpc}^{-1}$
$10^9 A_s$		...	$10^9\times$ dimensionless curvature power spectrum at $k_0 = 0.05\,\mathrm{Mpc}^{-1}$
$\omega_m \equiv \Omega_m h^2$		...	Total matter density today (inc. massive neutrinos)
z_*		...	Redshift for which the optical depth equals unity (see text)
$r_* = r_s(z_*)$		...	Comoving size of the sound horizon at $z = z_*$
$100\theta_*$		...	$100\times$ angular size of sound horizon at $z = z_*$ (r_*/D_A)
z_{drag}		...	Redshift at which baryon-drag optical depth equals unity (see text)
$r_{drag} = r_s(z_{drag})$		...	Comoving size of the sound horizon at $z = z_{drag}$
k_D		...	Characteristic damping comoving wavenumber (Mpc^{-1})
$100\theta_D$		...	$100\times$ angular extent of photon diffusion at last scattering (see text)
z_{eq}		...	Redshift of matter-radiation equality (massless neutrinos)
$100\theta_{eq}$		...	$100\times$ angular size of the comoving horizon at matter-radiation equality
$r_{drag}/D_V(0.57)$		...	BAO distance ratio at $z = 0.57$ (see Sect. 5.2)

[a] For dynamical dark energy models with constant equation of state, we denote the equation of state by w and adopt the same prior as for w_0.

The CMB polarization as a gravitational waves' detector

Scalar waves
(perturbation of the density)

Tensor waves
(perturbations of the metric)

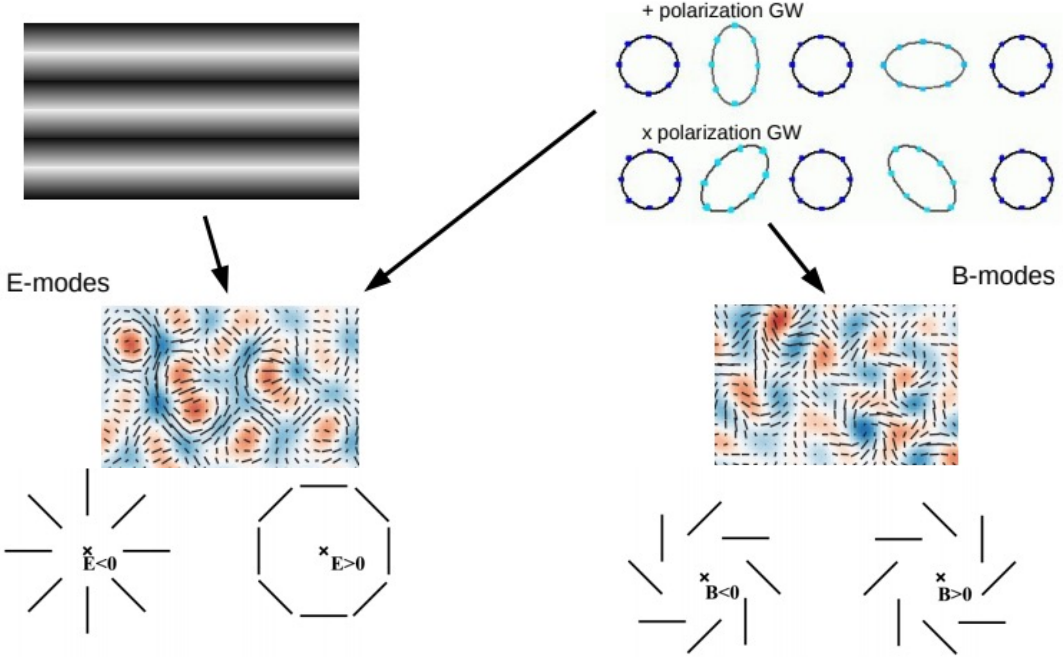

An **antisymmetric pattern** in the CMB polarization field can only be produced by tensor perturbations.
CMB polarization acts as a detector of primordial gravitational waves

Primordial perturbations and tensor-to-scalar ratio *r*

Primordial perturbations cab of 2 types (scalar and tensor)

$$\Delta^2_\zeta(k) = \Delta^2_\zeta \left(\frac{k}{k_*}\right)^{n_\mathrm{s}(k)-1} \quad \text{and} \quad \Delta^2_h(k) = \Delta^2_h \left(\frac{k}{k_\star}\right)^{n_\mathrm{t}(k)}$$

The tensor perturbation is related to inflation expansion rate

$$\Delta^2_h(k) = \frac{8}{M_P^2}\left(\frac{H}{2\pi}\right)^2 \qquad H = \left(\frac{\dot{a}}{a}\right)_{\text{inflation}}$$

The tensor-to-scalar ratio is the most relevant parameter to recover, related to energy scale of the inflation V (amplitude of the inflationary scalar filed)

$$r = \frac{\Delta^2_h(k)}{\Delta^2_\zeta(k)} \qquad V^{1/4} = 1.04 \times 10^{16}\mathrm{GeV}\left(\frac{r}{0.01}\right)^{1/4}$$

Tensor-to-scalar ratio: *r* parameter

CMB polarization acts as a detector of primordial gravitational waves

Primordial gravitational waves are seen as B-mode (antisymmetric patterns in CMB polarization);

The B-mode angular power spectrum at large angular scales (low-ell) is proportional to primordial GW

The primordial GW amplitude is expressed by the tensor-to-scalar ratio parameter: *r*

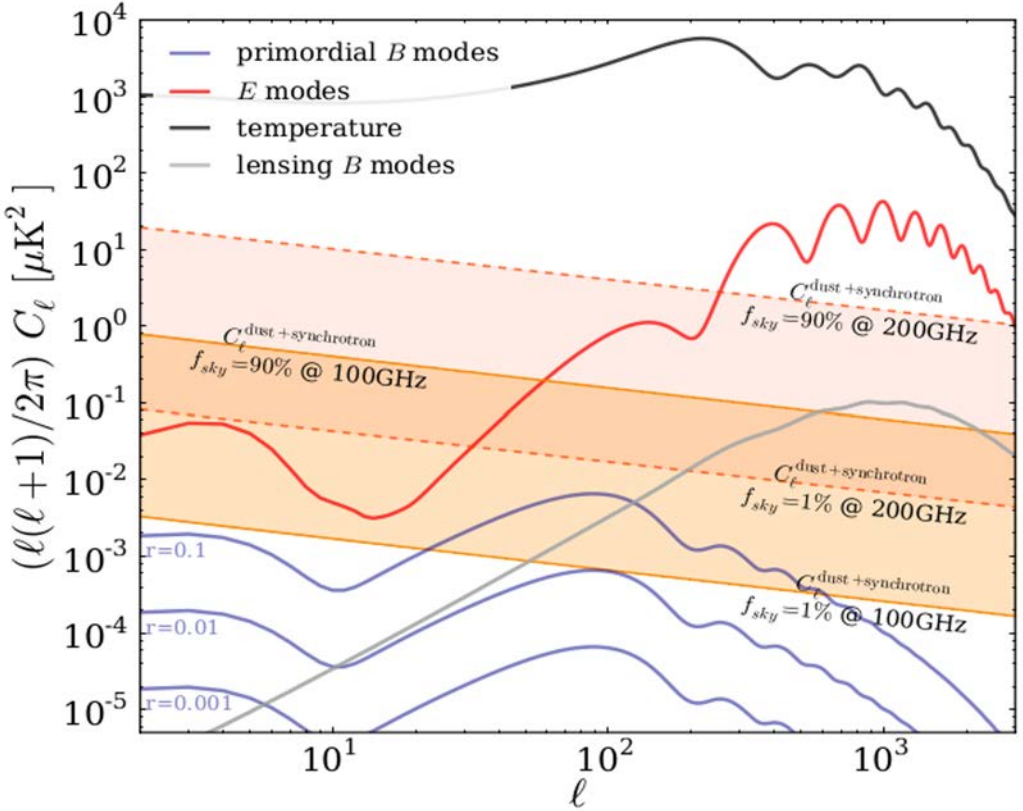

Tensor-to-scalar ratio: *r* parameter

CMB polarization acts as a detector of primordial gravitational waves

Primordial gravitational waves are seen as B-mode (antisymmetric patterns in CMB polarization);

The B-mode angular power spectrum at large angular scales (low-ell) is proportional to primordial GW

The primordial GW amplitude is expressed by the tensor-to-scalar ratio parameter: *r*

The primordial GW are due to inflationary phase in the very early Universe

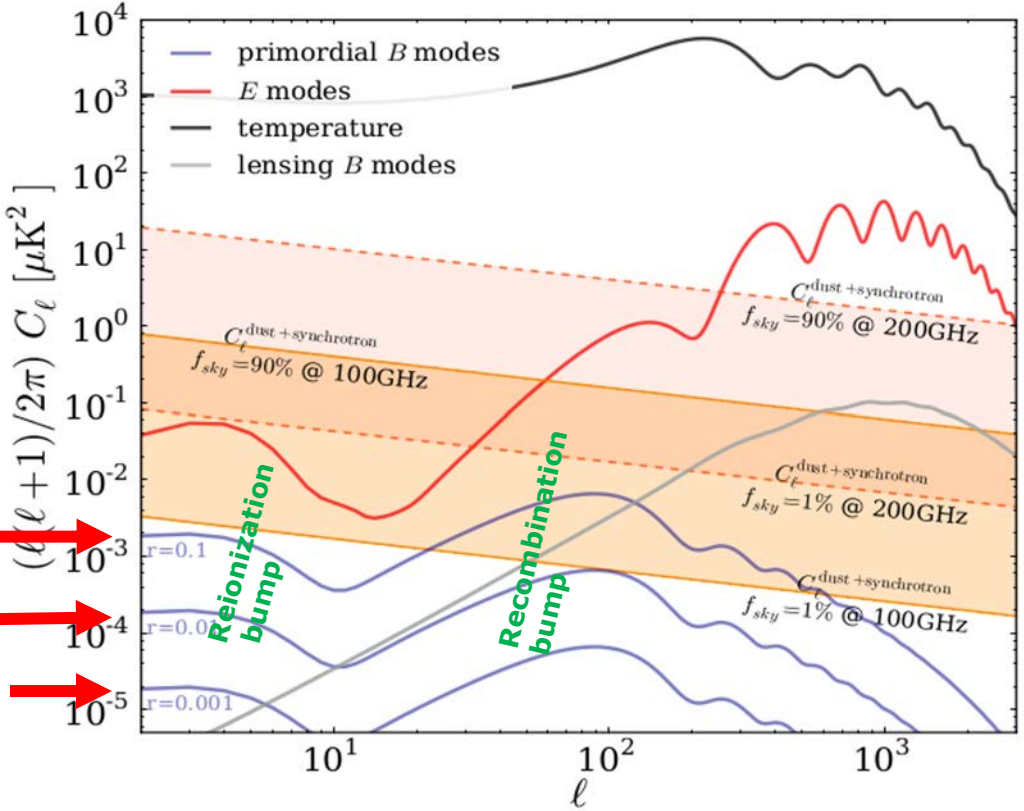

Status of measurements: B-mode angular power spectrum

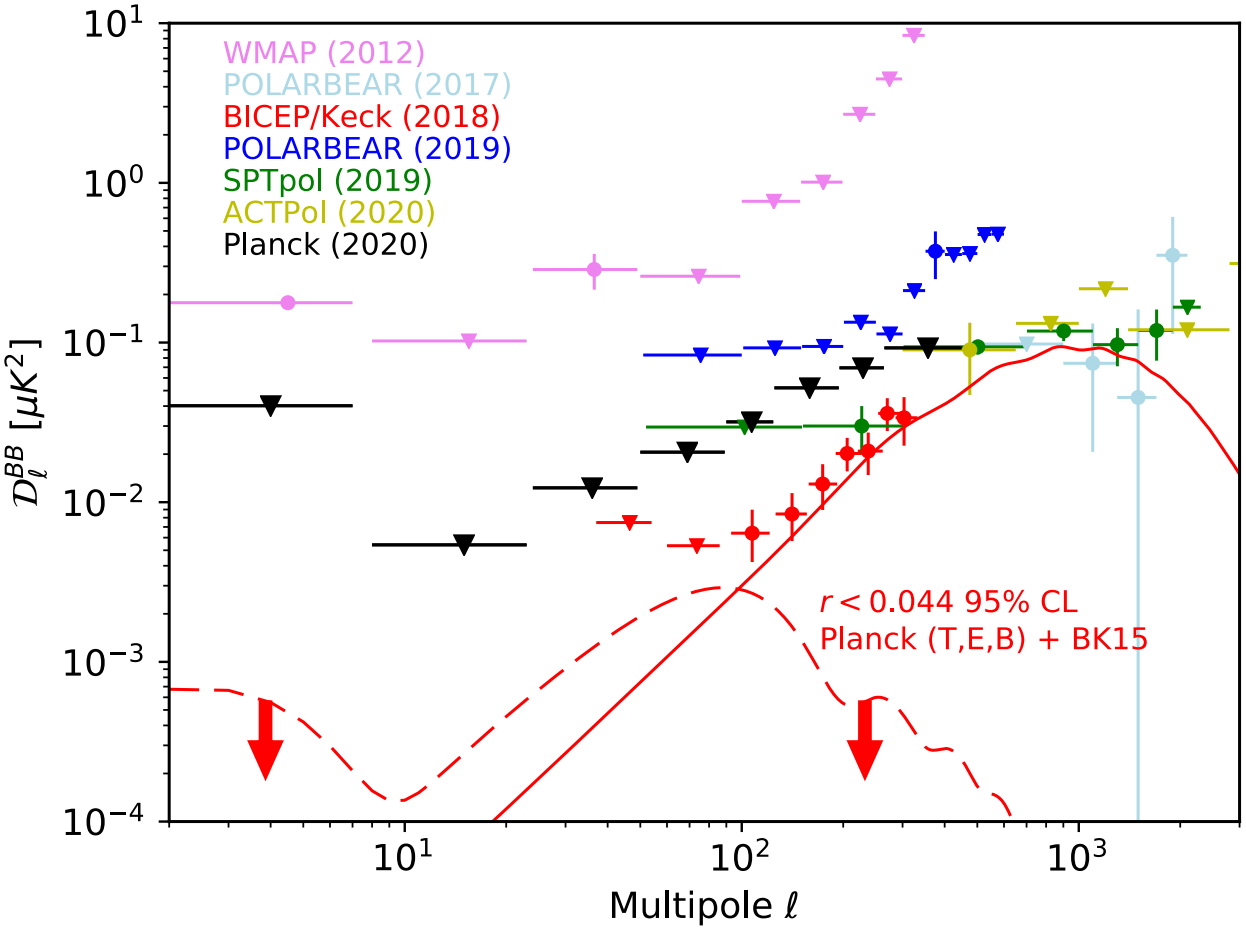

$r < 0.044$ 90%C.L.
(very indirect assessment)

From:
***Planck* constraints on the tensor-to-scalar ratio**
Tristram et al. A&A Vol. 647, March 2021
https://www.aanda.org/articles/aa/full_html/2021/03/aa39585-20/aa39585-20.html

Last update

PHYSICAL REVIEW LETTERS 127, 151301 (2021)

Improved Constraints on Primordial Gravitational Waves using Planck, WMAP, and BICEP/Keck Observations through the 2018 Observing Season

October 2021

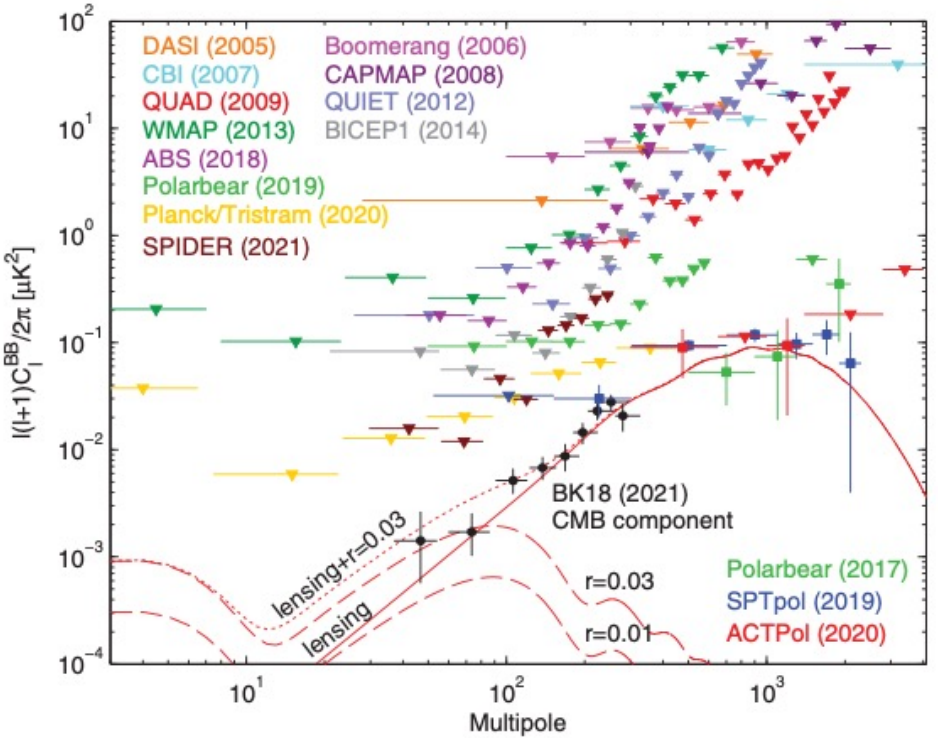

FIG. 7. Summary of CMB B-mode polarization upper limits [20,39,51–60] and detections [61–63]. Theoretical predictions are shown for the lensing B modes (solid red) that peak at arcminute scales (multipole $\ell \sim 1000$), and for gravitational wave B modes (dashed red) for two values of r peaking at degree scales ($\ell \sim 80$). The BK18 data are shown after removing Galactic foregrounds.

Last update

PHYSICAL REVIEW LETTERS 127, 151301 (2021)

Improved Constraints on Primordial Gravitational Waves using Planck, WMAP, and BICEP/Keck Observations through the 2018 Observing Season

October 2021

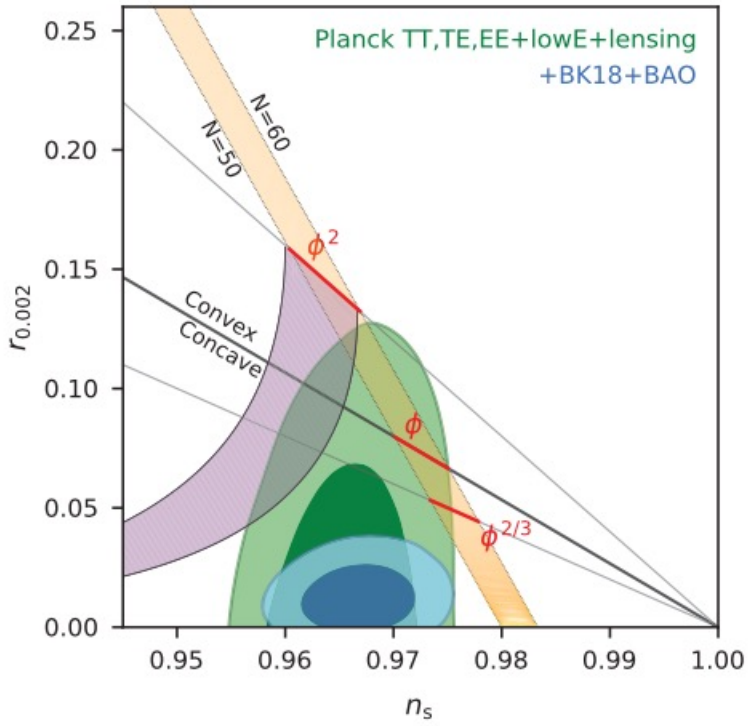

FIG. 5. Constraints in the r vs n_s plane for the *Planck* 2018 baseline analysis, and when also adding BICEP/*Keck* data through the end of the 2018 season plus BAO data to improve the constraint on n_s. The constraint on r tightens from $r_{0.05} < 0.11$ to $r_{0.05} < 0.035$. This figure is adapted from Fig. 28 of Ref. [2] with the green contours being identical. Some additional inflationary models are added from Fig. 8 of Ref. [50] with the purple region being natural inflation.

Main observational issues

Sensitivity $$\frac{\Delta T}{T_{\rm CMB}} \simeq \frac{30\,{\rm nK}}{2.7\,{\rm K}} = 10^{-8}$$

Foregrounds

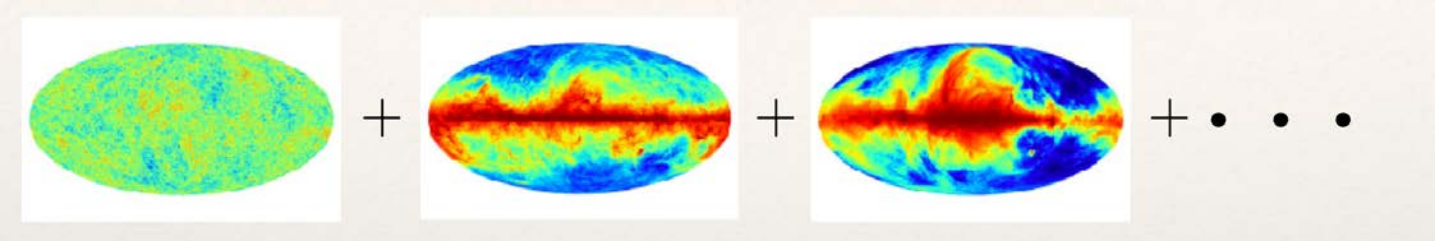

Systematic effects in measuring polarization

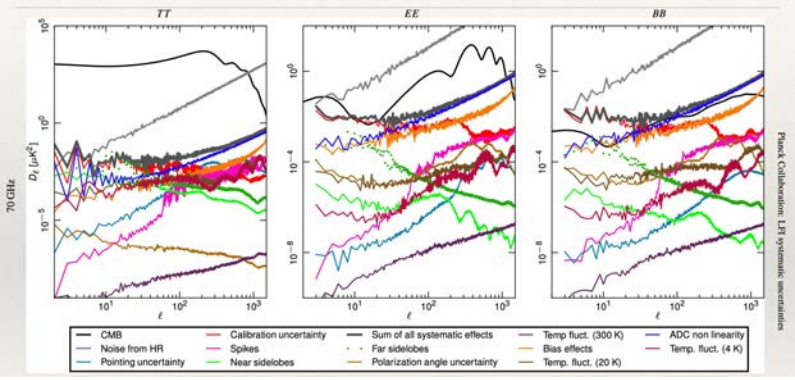

Sensitivity

Un-eliminable photon noise limits the sensitivity

- Intrinsic photon fluctuation of the 2.725 K CMB black body

Increasing the number of detectors and observation time

- Towards 100 000 detectors and more
- Years of data to be collected

Increasing the power on each detector

- Multimoded detectors (degrades optical response
- Wide frequency band (already very wide)

Thermal noise: 100-300 mK cryogenic systems

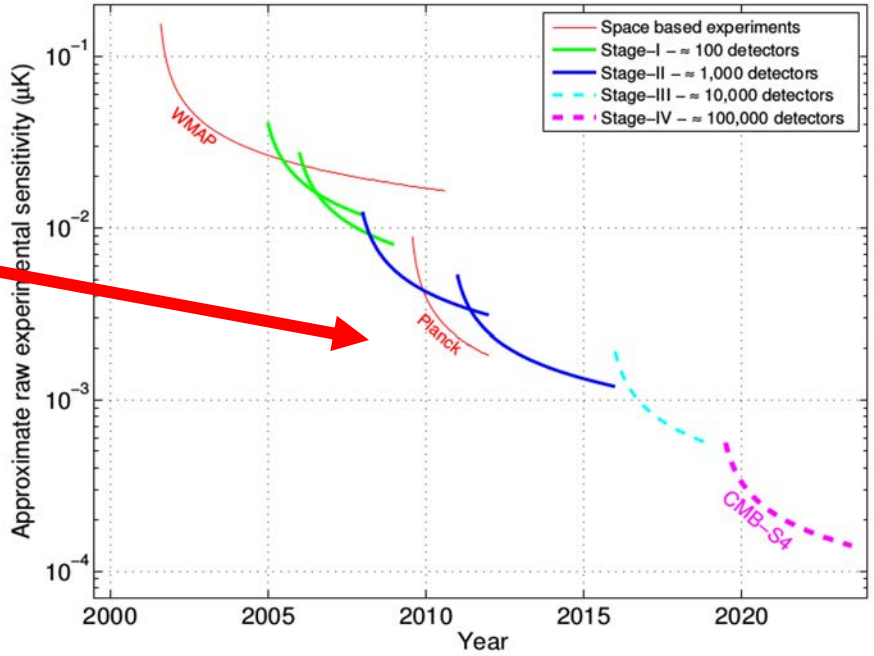

Foregrounds

We need to look through the Milky Way

In the microwave, relevant polarized emission by

Synchrotron radiation by electrons in the Milky Way

Interstellar Dust spinning in the magnetic field

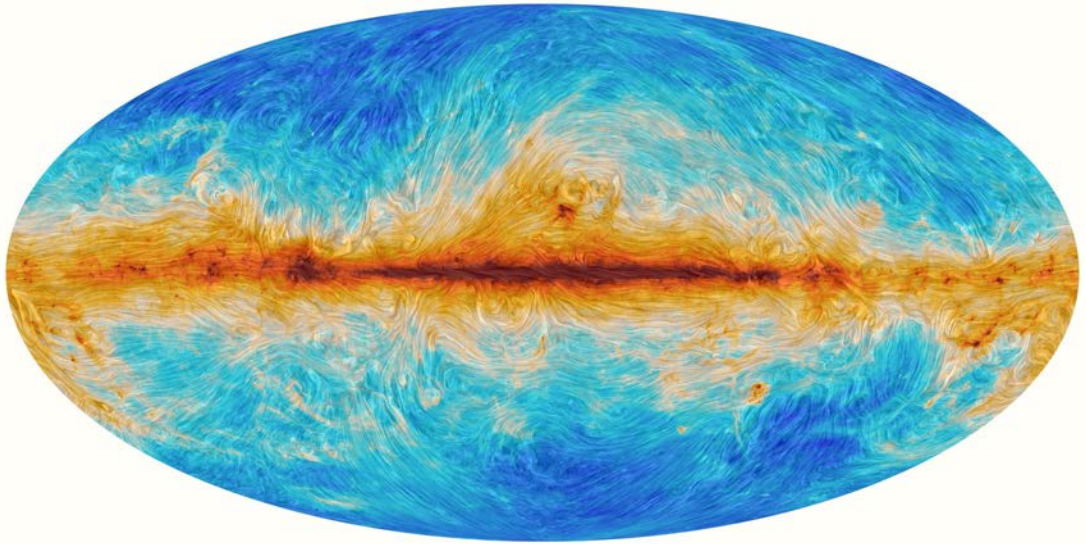

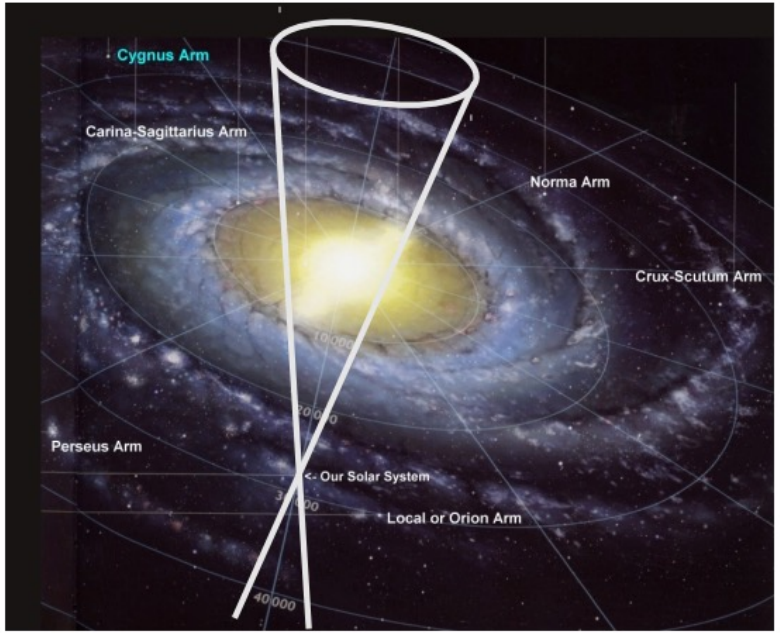

Foregrounds

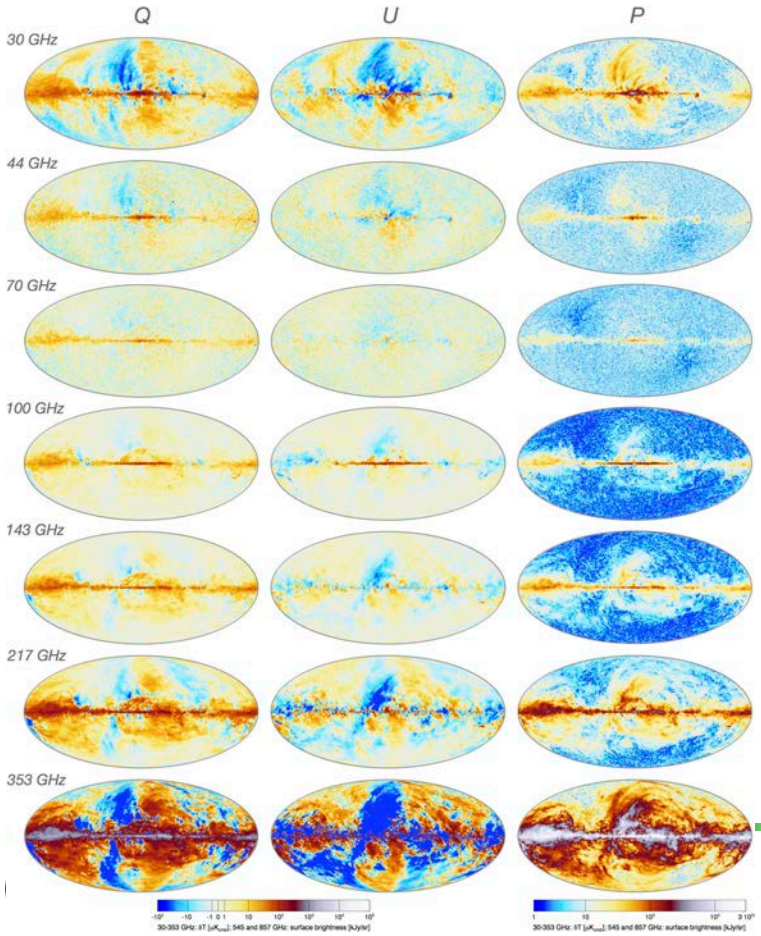

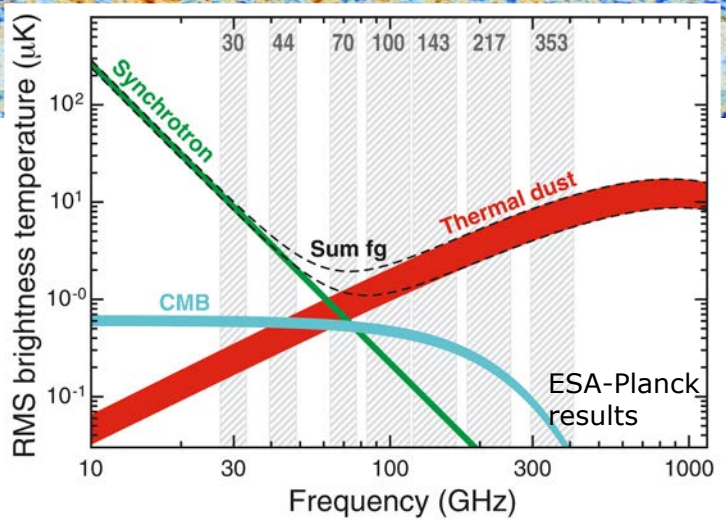

The CMB polarization signal (Q, U Stokes parameters) is almost completely foreground dominated

Foregrounds are different from CMB in terms of:

- Frequency dependance
- Spatial distribution (anisotropic)
- Statistical properties (non-Gaussian distribution)

With **observation in many bands** and **foreground modelling**, it is possible to disentangle CMB from foregrounds

ESA-Planck results

Systematic effects - modulation of the polarized component

Instrumental non-idealities can generate

- Polarization E-mode (~3 μK) to polarization B-mode (~30 nK) leakage
  - Factor 100 control
- CMB anisotropies (300 μK) to polarization B-mode leakage
  - Factor 10^4 control
- CMB dipole (3 mK) to polarization B-mode leakage
  - Factor 10^6 control
- CMB monopole (2.735 K) to polarization B-mode leakage
  - Factor 10^9 control

Systematic effects - modulation of the polarized component

Instrumental non-idealities can generate

- Polarization E-mode (~3 μK) to polarization B-mode (~30 nK) leakage
  - Factor 100 control
- CMB anisotropies (300 μK) to polarization B-mode leakage
  - Factor 10^4 control
- CMB dipole (3 mK) to polarization B-mode leakage
  - Factor 10^6 control
- CMB monopole (2.735 K) to polarization B-mode leakage
  - Factor 10^9 control

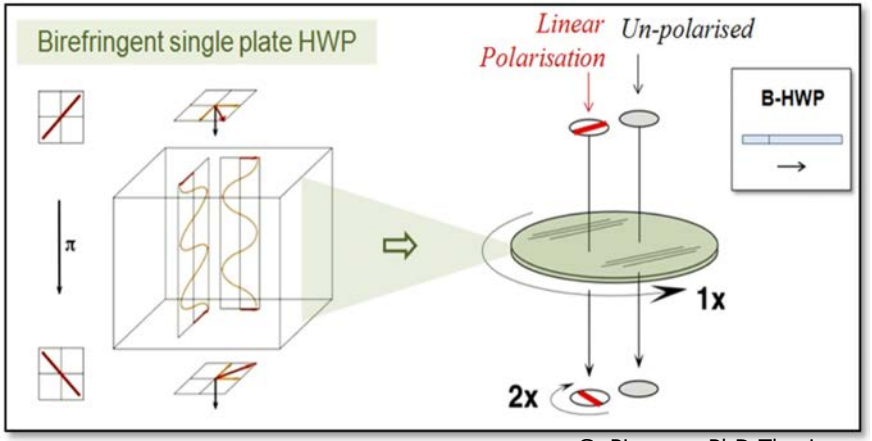

G. Pisano – PhD Thesis

Polarization Modulation Unit:

- Spinning birefringent **Half Wave Plate + polarization selector** modulates polarized radiation only
- Rejects most of the systematic effects (polarized signal is modulated at 4x the spinning frequency)
- It comes to a cost
  - Must be cooled (~10K) to avoid emission issues, and spin (cold) at constant speed (~1 Hz)
  - Must be broadband
  - Can introduce extra systematic effects

International effort

The US plays a major role in leading ground-based Southern hemisphere instruments

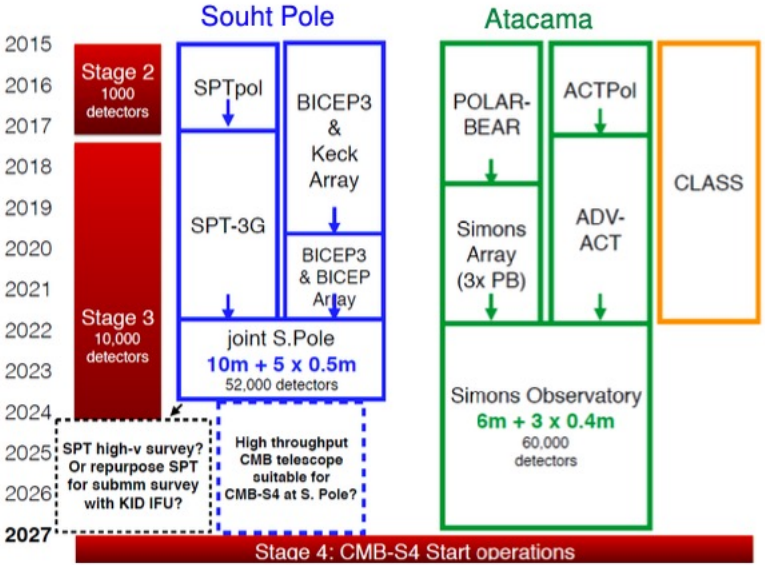

Credit M. Bersanelli

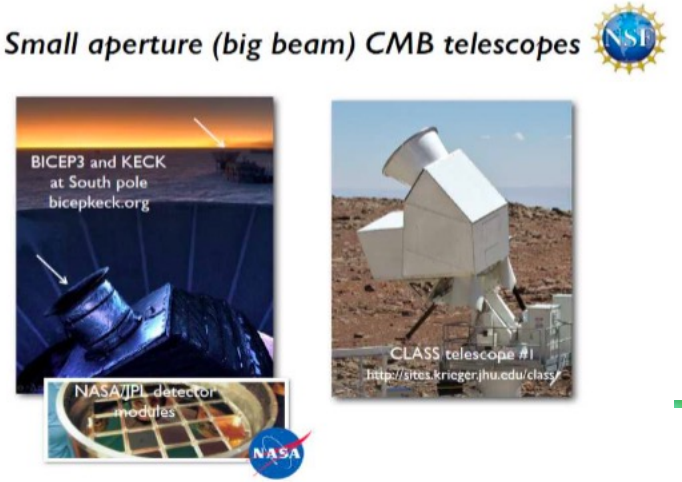

Focus: LSPE balloon/ground-based

Large Scale Polarizarion Explorer – 2 independent instruments:

https://iopscience.iop.org/article/10.1088/1475-7516/2021/08/008/meta
The LSPE Collaboration, JCAP 08(2021)008, 2021

Focus: LSPE balloon/ground-based

Large Scale Polarizarion Explorer – 2 independent instruments:

Strip – Ground-based in Tenerife

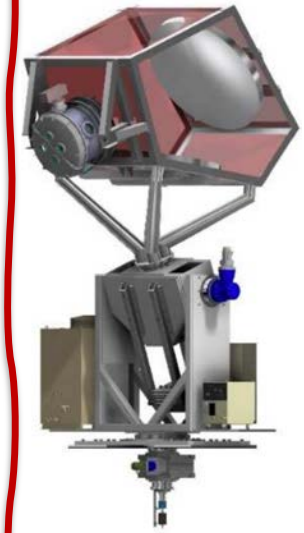

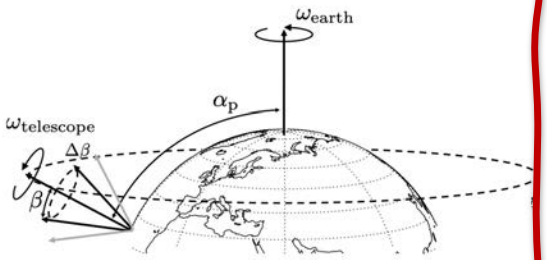

Radiometers at
43 GHz control of synchrotron FG
95 GHz control of atmosphere

PI: **M. Bersanelli** (University of Milam)

https://iopscience.iop.org/article/10.1088/1475-7516/2021/08/008/meta
The LSPE Collaboration, JCAP 08(2021)008, 2021

Focus: LSPE balloon/ground-based

Large Scale Polarizarion Explorer – 2 independent instruments:

Strip – Ground-based in Tenerife

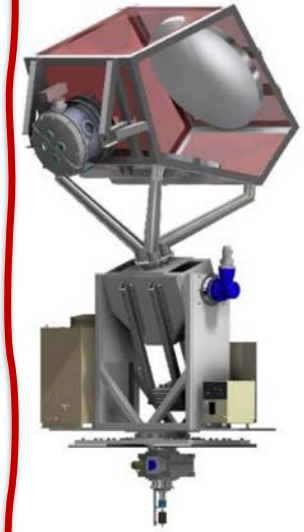

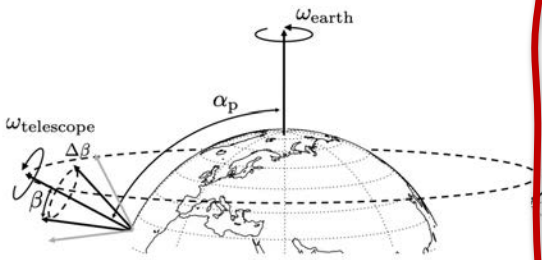

Radiometers at

43 GHz	control of synchrotron FG
95 GHz	control of atmosphere

PI: **M. Bersanelli** (University of Milam)

SWIPE – winter arctic long duration balloon

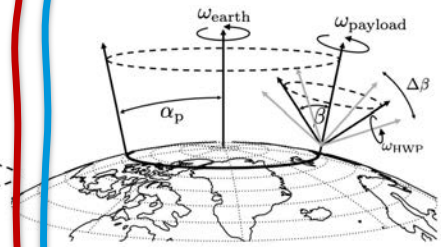

Multimoded TES bolometers at

145 GHz	CMB
210 GHz	Dust FG
240 GHz	Atm

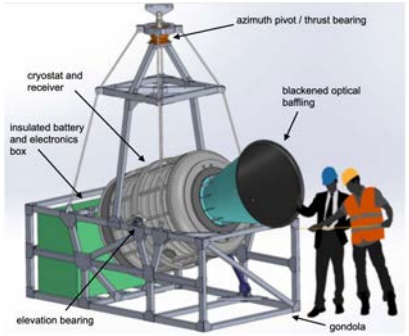

Figure 11. LSPE-SWIPE overview. The instrument is contained in a large liquid Helium cryostat, which al
contains the optical elements, including the HWP based Stokes polarimeter. The on-board electronics and
Lithium batteries based power system are contained in an Aerogel insulated box, to optimize thermal balan

PI: **P. de Bernardis** (Sapienza University of Rome)

https://iopscience.iop.org/article/10.1088/1475-7516/2021/08/008/meta
The LSPE Collaboration, JCAP 08(2021)008, 2021

Focus: LSPE balloon/ground-based - sensitivity

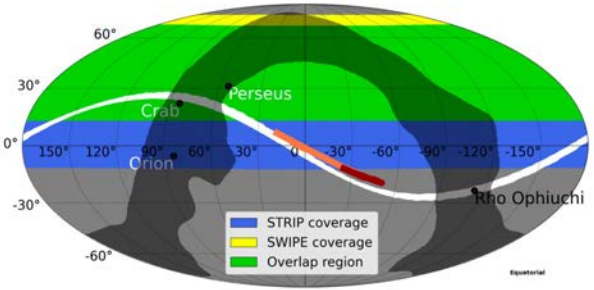

Figure 3. Map in Equatorial coordinates of the Strip-SWIPE coverage. The yellow area represents the SWIPE sky coverage; the blue area represents the Strip sky coverage, in the case of 35°zenith angle; the green area shows the overlap and the grey area represent a Galactic mask that covers 30% of the whole sky. The Strip-coverage ranges from -7 to 63°in latitude, and the SWIPE coverage from 13 to 77°. The map also shows the position of the Crab and Orion nebula, of the Perseus molecular cloud and the trajectories of Jupiter (orange), Saturn (dark red) and the Moon (white) from April 2021 to April 2023.

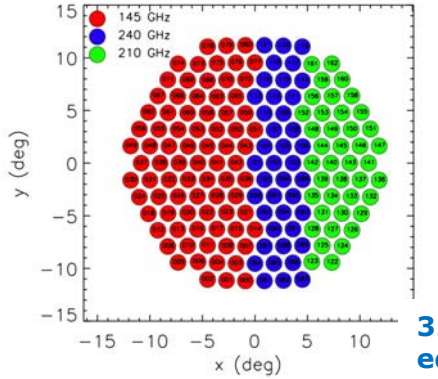

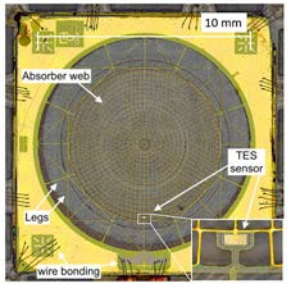

326 multimoded detectors total, equivalent to ~7000 single mode detectors

https://iopscience.iop.org/article/10.1088/1475-7516/2021/08/008/meta
The LSPE Collaboration, JCAP 08(2021)008, 2021

Focus: LSPE balloon/ground-based - sensitivity

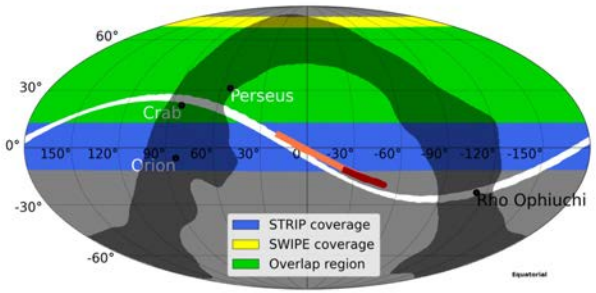

Figure 3. Map in Equatorial coordinates of the Strip-SWIPE coverage. The yellow area represents the SWIPE sky coverage; the blue area represents the Strip sky coverage, in the case of 35°zenith angle; the green area shows the overlap and the grey area represent a Galactic mask that covers 30% of the whole sky. The Strip-coverage ranges from -7 to 63°in latitude, and the SWIPE coverage from 13 to 77°. The map also shows the position of the Crab and Orion nebula, of the Perseus molecular cloud and the trajectories of Jupiter (orange), Saturn (dark red) and the Moon (white) from April 2021 to April 2023.

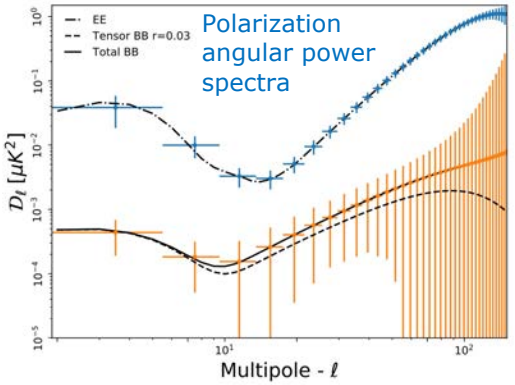

Polarization angular power spectra

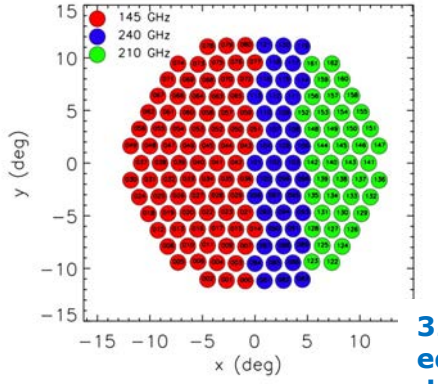

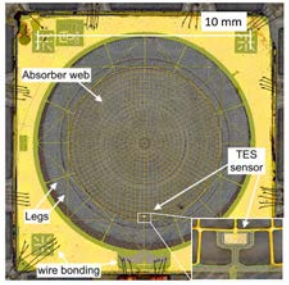

326 multimoded detectors total, equivalent to ~7000 single mode detectors

r posterior probability

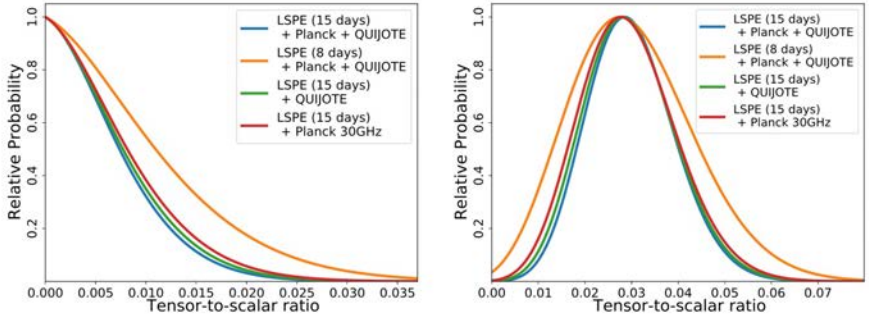

Figure 26. Posterior probability for tensor-to-scalar ratio r in case of $r = 0$ (*left*) and $r = 0.03$ (*right*). The colored lines show different component separation configurations, see text for details.

https://iopscience.iop.org/article/10.1088/1475-7516/2021/08/008/meta
The LSPE Collaboration, JCAP 08(2021)008, 2021

Focus: LSPE balloon/ground-based - sensitivity

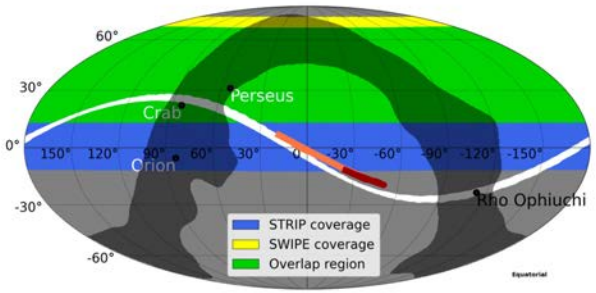

Figure 3. Map in Equatorial coordinates of the Strip-SWIPE coverage. The yellow area represents the SWIPE sky coverage; the blue area represents the Strip sky coverage, in the case of 35°zenith angle; the green area shows the overlap and the grey area represent a Galactic mask that covers 30% of the whole sky. The Strip-coverage ranges from -7 to 63°in latitude, and the SWIPE coverage from 13 to 77°. The map also shows the position of the Crab and Orion nebula, of the Perseus molecular cloud and the trajectories of Jupiter (orange), Saturn (dark red) and the Moon (white) from April 2021 to April 2023.

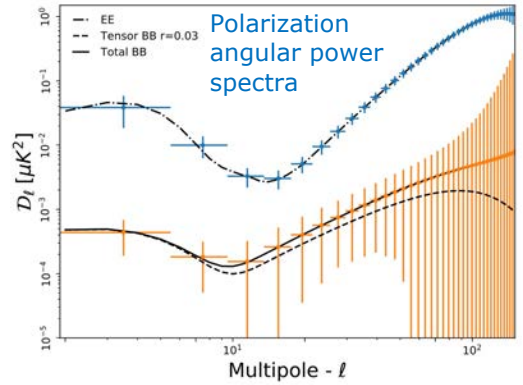

Estimated sensitivity
$\delta r = 0.01$

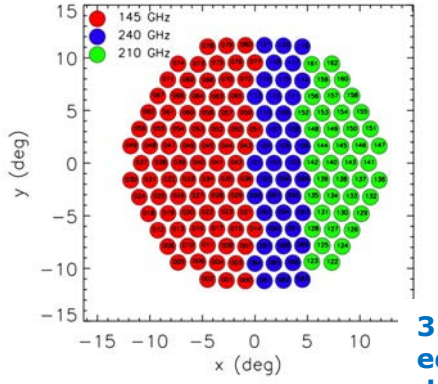

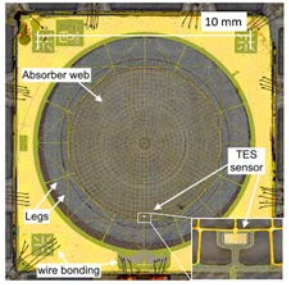

326 multimoded detectors total, equivalent to ~7000 single mode detectors

***r* posterior probability**

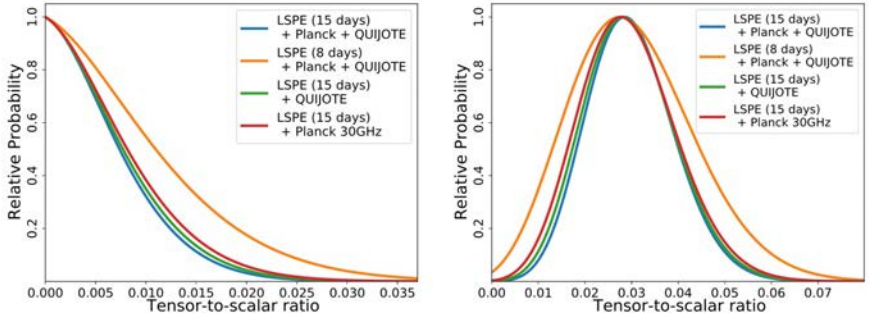

Figure 26. Posterior probability for tensor-to-scalar ratio r in case of $r = 0$ (*left*) and $r = 0.03$ (*right*). The colored lines show different component separation configurations, see text for details.

https://iopscience.iop.org/article/10.1088/1475-7516/2021/08/008/meta
The LSPE Collaboration, JCAP 08(2021)008, 2021

Focus: LSPE balloon/ground-based - systematic effects control

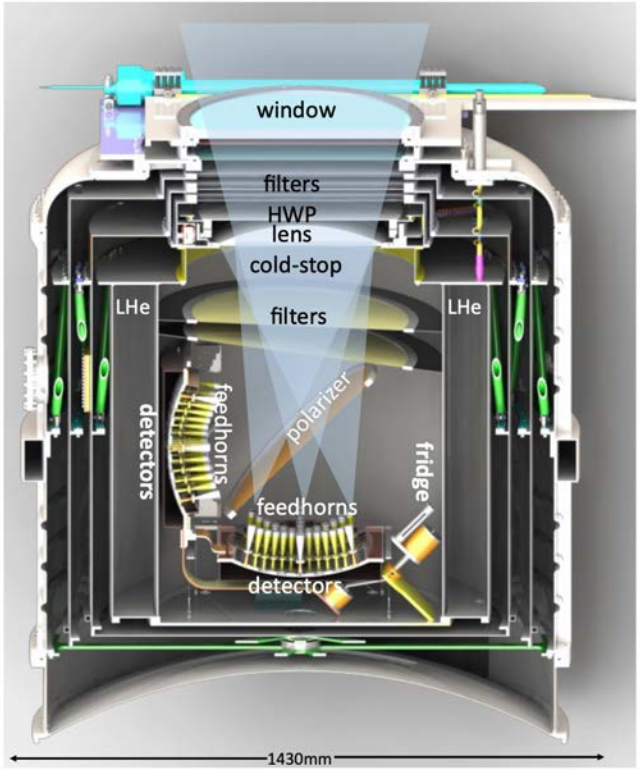

Polarization modulation Unit

- Cryogenic rotating Half-Wave Plate
- Transmissive Half-Wave Plate
- 500 mm diameter
- 4K magnetically levitating superconductive bearing
- Launch-lock clamp system
- Fiber-optics based encoder + Kalman filter-based readout

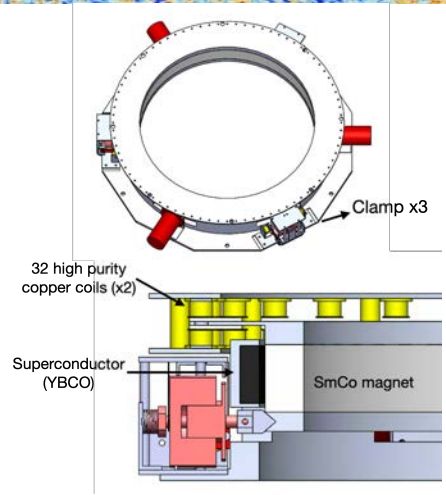

LSPE-SWIPE Parameter	Requirement	B-mode (r.m.s.)	reference
Instrumental polarization[1,2]	$< 4 \times 10^{-4}$	$18\,\mathrm{nK_{CMB}}$	4.3.1
Cross polarization[2]	< 0.02	$10\,\mathrm{nK_{CMB}}$	4.3.1
Polarization angle recovery	$< 40'$	$12\,\mathrm{nK_{CMB}}$	4.3.2
WG angle error	$\Delta\phi_{\mathrm{WG}} < 20'$	$6\,\mathrm{nK_{CMB}}$	4.3.2, 4.3.3
HWP angle offset	$\Delta\theta_{\mathrm{HWP}} < 10'$	$6\,\mathrm{nK_{CMB}}$	4.3.2, 4.3.3
HWP angle noise	$\sigma_{\theta_{\mathrm{HWP}}} < 10'$	$6\,\mathrm{nK_{CMB}}$	4.3.2, 4.3.3
Time constant knowledge[2]	$\Delta\tau_{\mathrm{LP}} < 1.0\,\mathrm{ms}$	$6\,\mathrm{nK_{CMB}}$	4.3.2, 4.3.3
HWP angular velocity measurement	$\sigma_{\omega_{\mathrm{HWP}}}/\omega_{\mathrm{HWP}} < 5 \times 10^{-6}$	$6\,\mathrm{nK_{CMB}}$	4.3.3
Mueller matrix $I \to Q/U$ terms knowledge	$\Delta M_{IQ}^{4\theta}, \Delta M_{IU}^{4\theta} < 10^{-4}$	$6\,\mathrm{nK_{CMB}}$	[111, 112]

https://iopscience.iop.org/article/10.1088/1475-7516/2021/08/008/meta
The LSPE Collaboration, JCAP 08(2021)008, 2021

LiteBIRD Joint Study Group

Over 300 researchers from **Japan**, **North America** and **Europe**

Team experience in CMB experiments, X-ray satellites and other large projects (ALMA, HEP experiments, …)

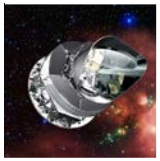



LiteBIRD Global F2F meeting
December 11-13, 2019 at MPE

LiteBIRD overview

- Lite (Light) satellite for the study of *B*-mode polarization and Inflation from cosmic background Radiation Detection
- JAXA's L-class mission selected in May 2019
- Expected launch in late **2029** with JAXA's H3 rocket
- **All-sky 3-year survey**, from Sun-Earth Lagrangian point L2
- Large frequency coverage (**40–402 GHz**, 15 bands) at **70–18 arcmin** angular resolution for precision measurements of the **CMB *B*-modes**
- Final combined sensitivity: **2.2 μK·arcmin**, after component separation

📖 Hazumi+ SPIE 2020

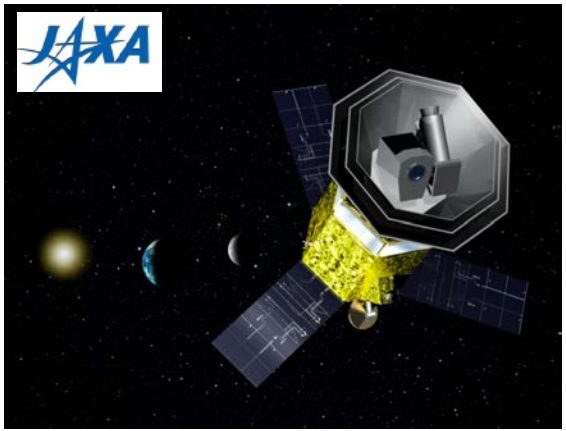

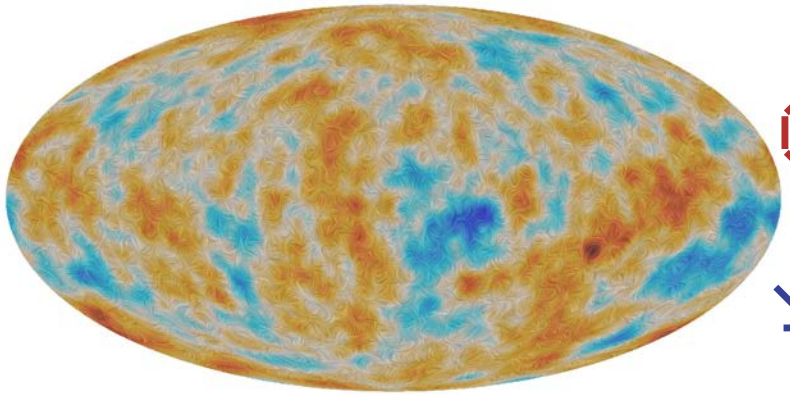

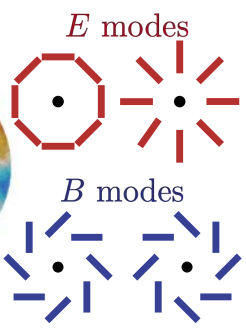

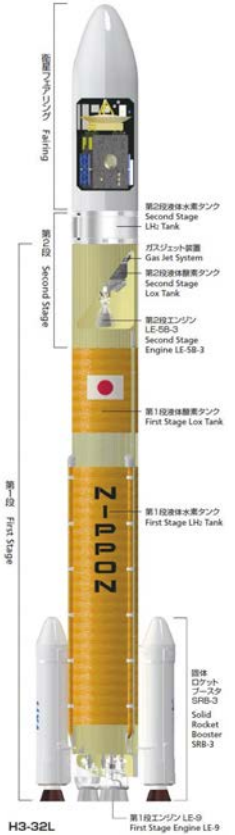

LiteBIRD main scientific objectives

- Definitive search for the ***B*-mode signal** from **cosmic inflation** in the CMB polarization
  - Making a discovery or ruling out well-motivated inflationary models
  - Insight into the quantum nature of gravity
- The inflationary (i.e. primordial) *B*-mode power is proportional to the **tensor-to-scalar ratio, *r***

Current best constraint: $r < 0.044$ (95% C.L.)
(📖 Tristram+ A&A 2021)

- LiteBIRD will improve current sensitivity on *r* by a factor ~50
- L1-requirements (no external data):
  - For $r = 0$, **total uncertainty of $\delta r < 0.001$**
  - For $r = 0.01$, 5-σ detection of the reionization ($2 < \ell < 10$) and recombination ($11 < \ell < 200$) peaks independently
- Huge discovery impact (evidence for inflation, knowledge of its energy scale, …)

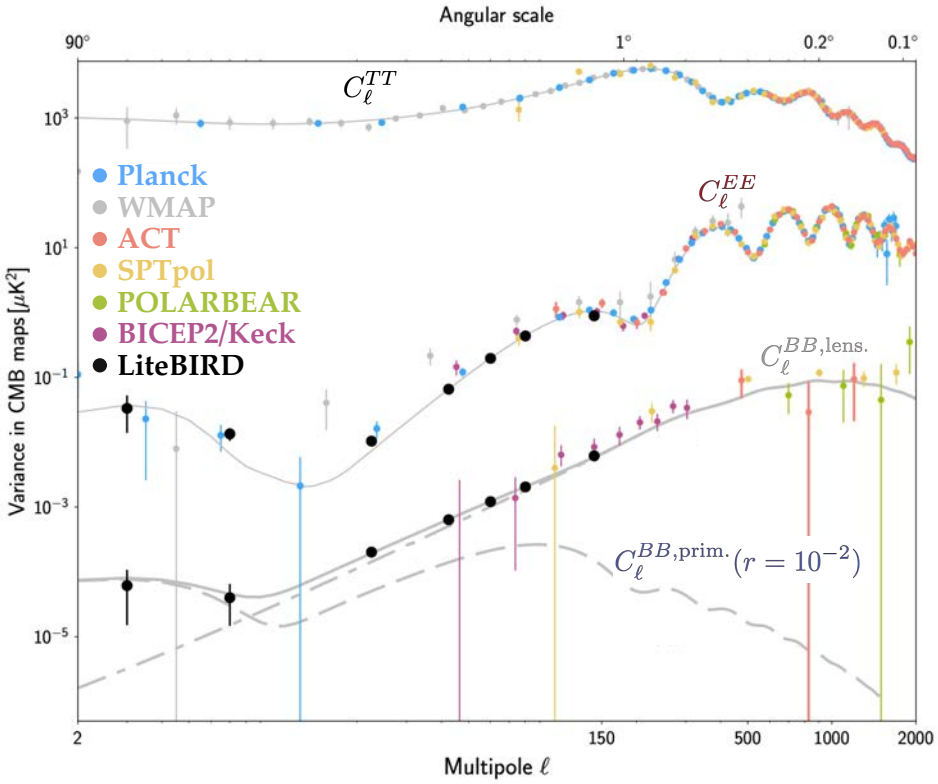

LiteBIRD other science outcomes

- The mission specifications are driven by the required sensitivity on r
- Meeting those sensitivity requirements would allow to address other important scientific topics, such as:

1. Characterize the B-mode power spectrum and search for source fields (e.g. scale-invariance, non-Gaussianity, parity violation, …)
2. Power spectrum features in polarization
   - Large-scale ***E*-modes**
   - **Reionization** (improve $\sigma(\tau)$ by a factor of 3)
   - **Neutrino mass** ($\sigma(\sum m_\nu) = 15$ meV)
3. Constraints on **cosmic birefringence**
4. **SZ effect** (thermal, diffuse, relativistic corrections)
5. Elucidating **anomalies**
6. **Galactic science**
   - Characterizing the foreground SED
   - Large-scale Galactic magnetic field
   - Models of dust polarization

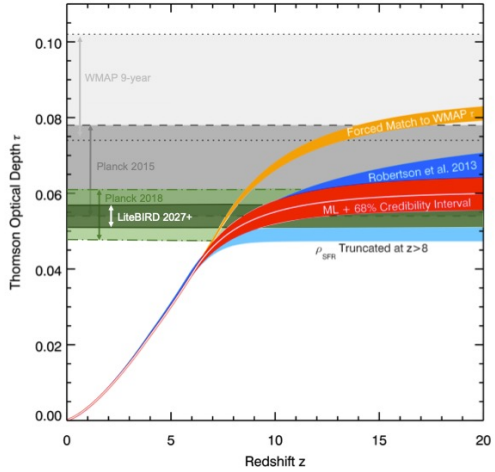

adapted from Robertson+2015

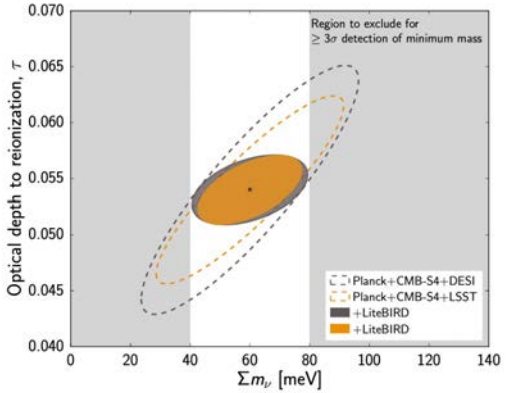

adapted from Calabrese+2017

LiteBIRD scanning strategy

- 3-year survey, Sun-Earth L2 Lissajous orbit
- Precession angle: $\alpha = 45°$
- Spin angle: $\beta = 50°$

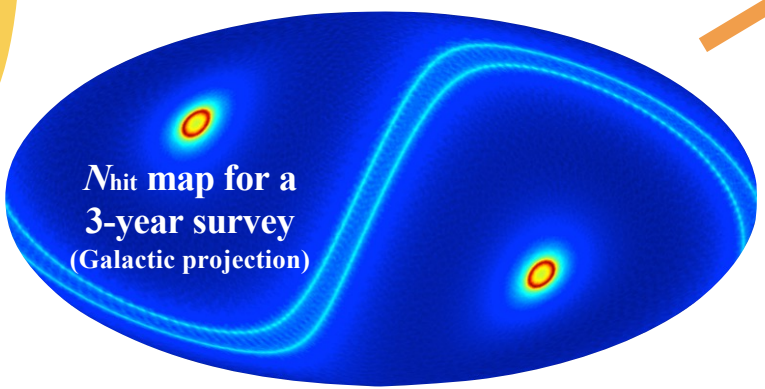

N_{hit} **map for a 3-year survey**
(Galactic projection)

LiteBIRD spacecraft overview

- **3 telescopes** are used to provide the **40-402 GHz** frequency coverage
  1. **LFT** (low frequency telescope)
  2. **MFT** (middle frequency telescope)
  3. **HFT** (high frequency telescope)
- Multi-chroic transition-edge sensor (TES) **bolometer arrays** cooled to **100 mK**
- Polarization modulation unit (PMU) in each telescope with **rotating half-wave plate** (HWP), for 1/*f* noise and systematics reduction
- Optics cooled to **5 K**

- Mass: 2.6 t
- Power: 3.0 kW
- Data: 17.9 Gb/day

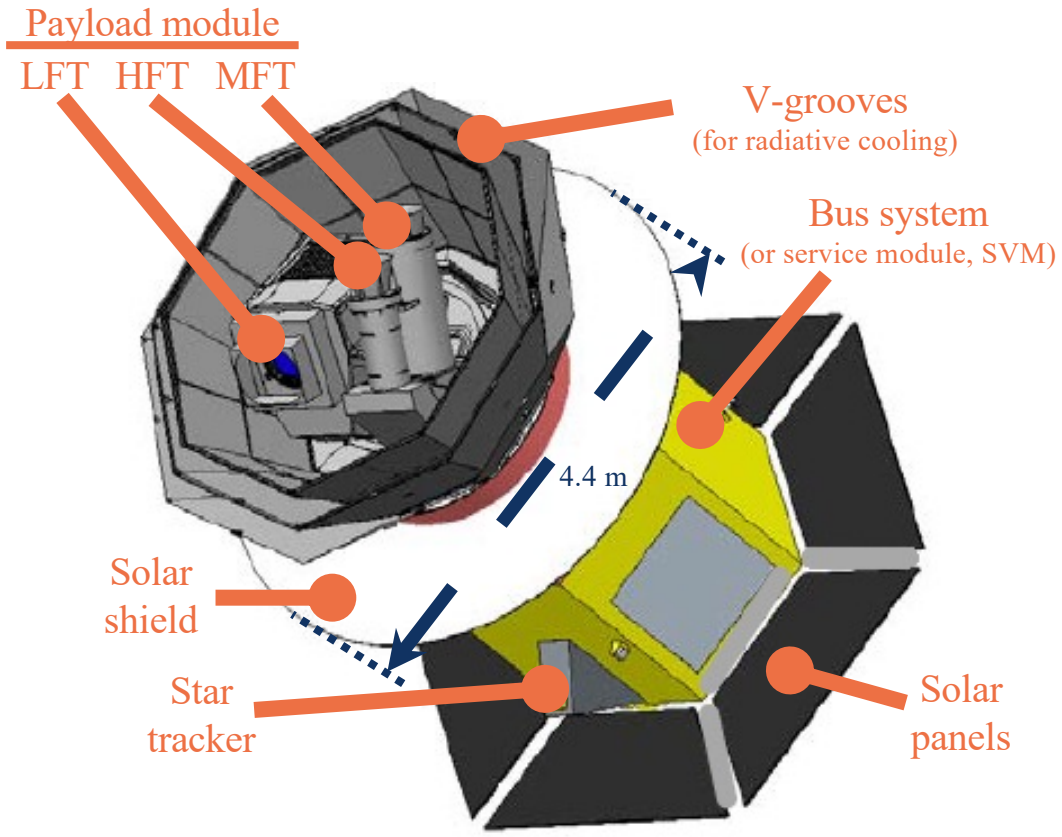

Low Frequency Telescope (LFT)

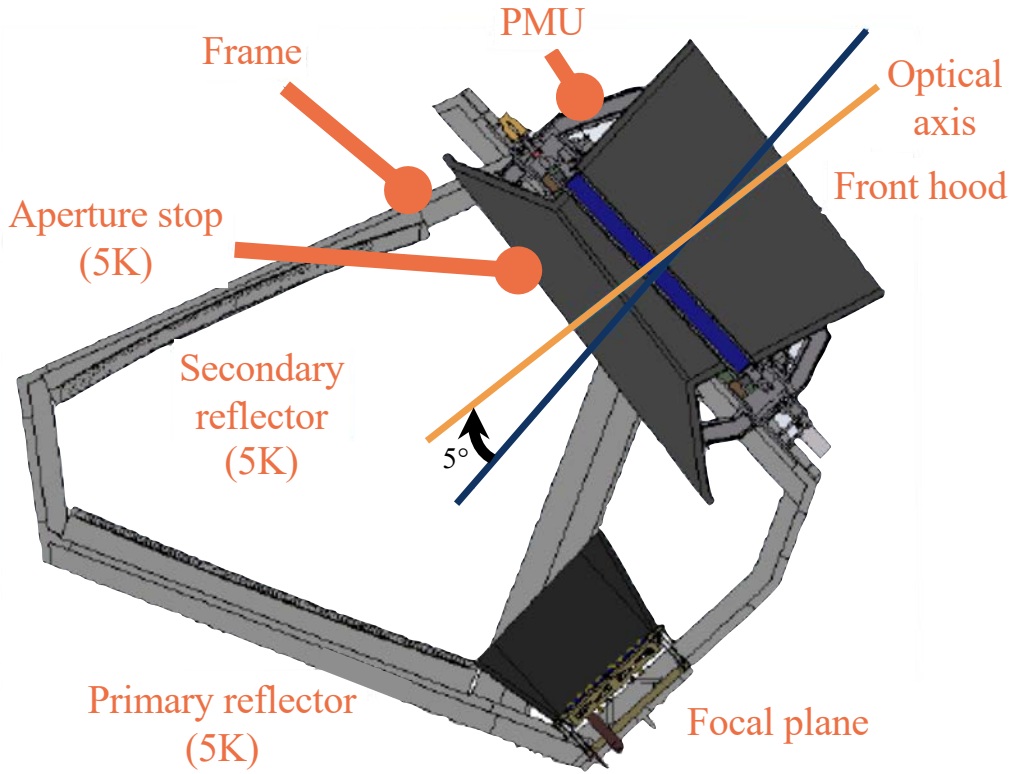

- Polarization Modulation Unit (PMU) as the first sky-side optical element
- **Crossed-Dragone** design
  - Mirrors and aperture stop at **5 K**
  - Made of aluminium
- Field of view: **18°×9°**
- Strehl ratio > 0.95 (@ 140 GHz)
- Aperture diameter: **400 mm**
- Frequency range: **40-140 GHz**
- Angular resolution: **70-24 arcmin**
- F#3.0 & cross angle of 90°
- Cross-polarization < **-30 dB**
- Rotation of the polarization angle across the FoV < ±1.5°
- Weight < 200 kg

Sekimoto+ SPIE 2020

Middle-High Frequency Telescopes (MFT/HFT)

Montier+ SPIE 2020

Lamagna+ SPIE 2020

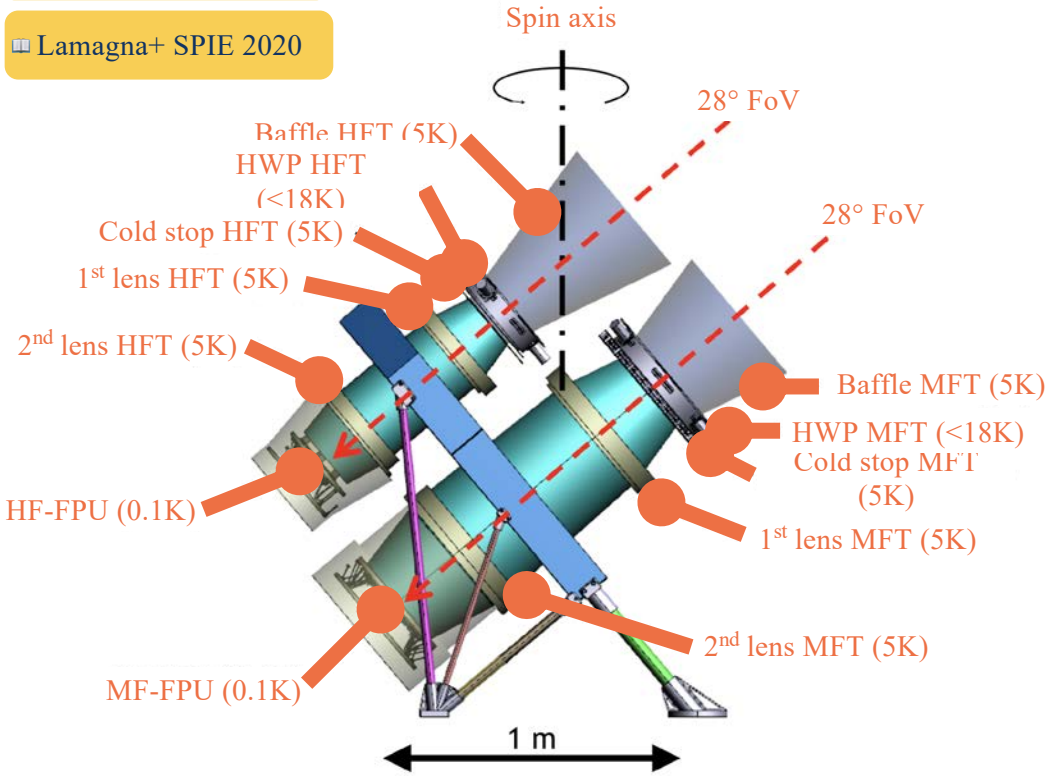

- Refractive optics
- Each telescope has PMU with a half-wave-plate (HWP)
- Optics at **5 K**
- Field of view: **28°**
- Simple and high heritage from ground experiments
- Compact (mass & volume)
- Simplified design for filtering scheme
- HDPE lenses + ARC
- Weight 100 kg

	MFT	HFT
ν (GHz)	**100-195**	**195-402**
Ap. diameter (mm)	**300**	**200**
Ang. res. (arcmin)	**38-28**	**29-18**

Focal plane configuration

- Transition-Edge Sensor (TES) arrays

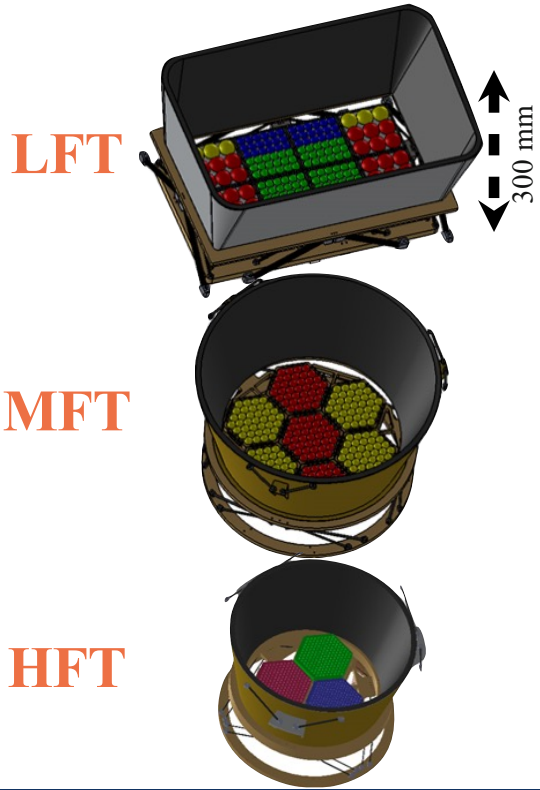

	LFT	MFT	HFT
Detector type	Lenslet/sinous	Lenslet/sinous	Horn/OMT
Nbands	9 (40-140 GHz)	5 (100-195 GHz)	5 (195-402 GHz)
Ndet	1080	2074	1354

Lensed coupled detectors

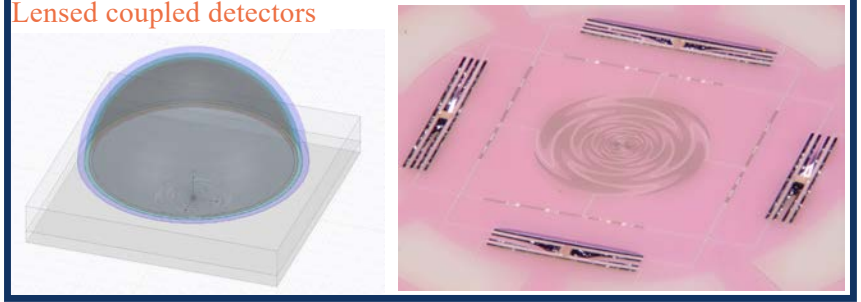

Horn-coupled detectors

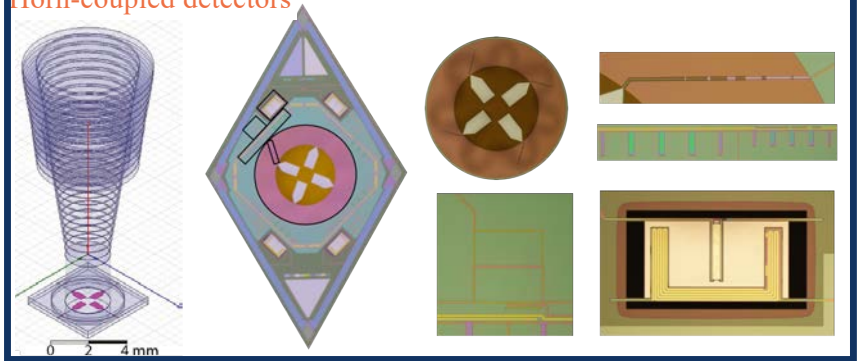

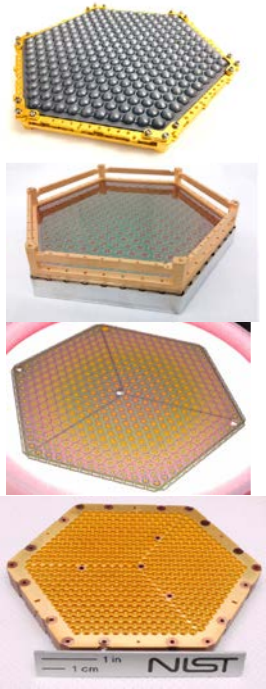

Westbrook+ SPIE 2020

LiteBIRD sensitivities

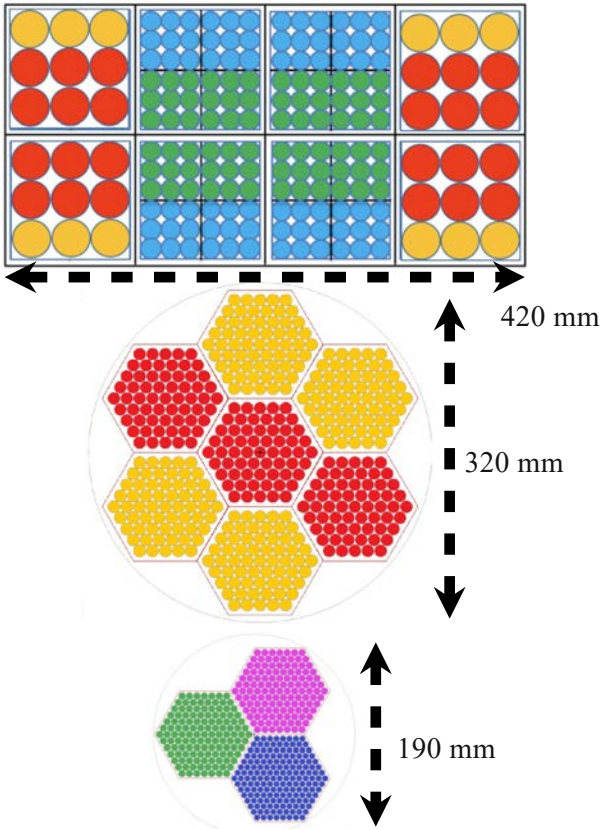

Telescope	Detector type	Module	Frequency [GHz]	Pixel size [mm]	Module count	Pixel count	Detector count
LFT	Lenslet/ Sinuous	LF12	40/60/78	32	4	24	144
			50/68/89	32		12	72
		LF34	68/89/119	16	4	72	432
			78/100/140	16		72	432
				Total LFT	8	180	1080
MFT	Lenslet/ Sinuous	MF1	100/140/195	12	3	183	1098
		MF2	119/166	12	4	244	976
				Total MFT	7	607	2074
HFT	Horn/ OMT	HF1	195/280	7	1	127	508
		HF2	235/337	7	1	127	508
		HF3	402	6.1	1	169	338
				Total HFT	3	423	1354
				Total mission	18	1210	4508

LiteBIRD sensitivities

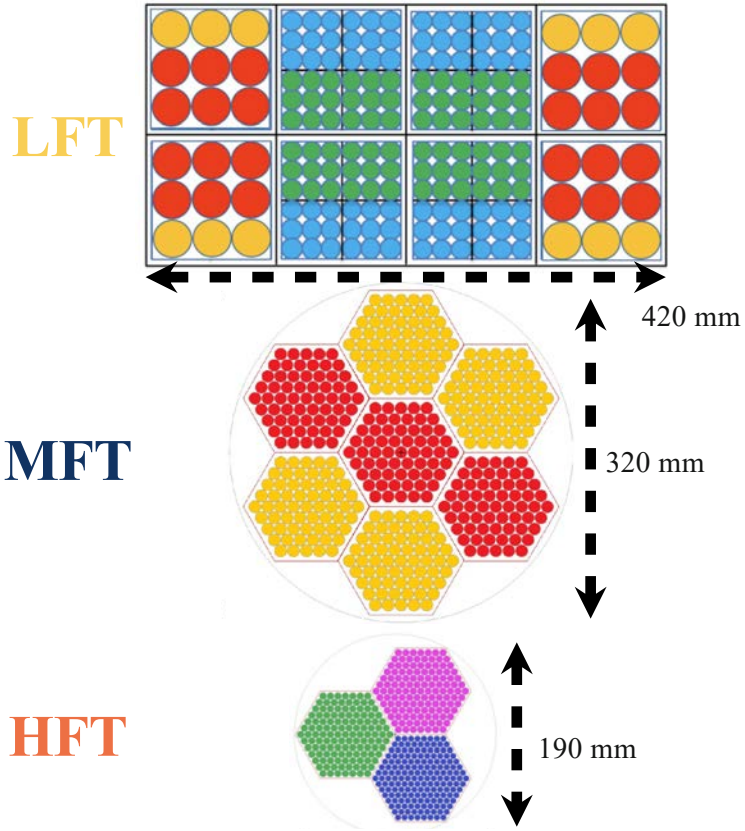

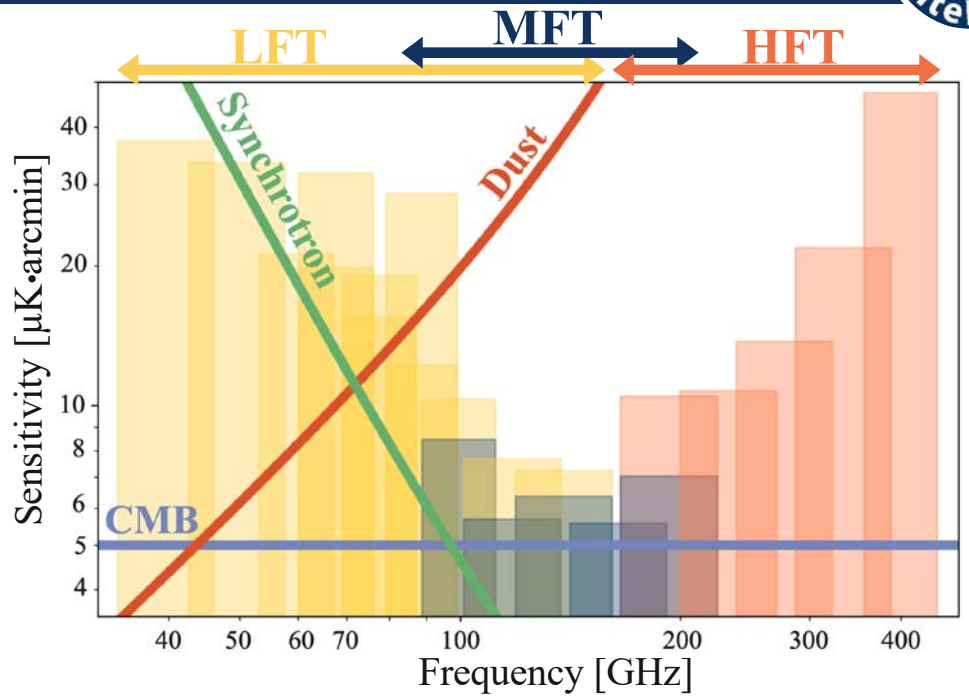

- Projected **polarization sensitivities** for a **3-year full-sky survey**
- Best of 4.3 μK·arcmin @ 119 GHz (Hazumi+ 2020)
- Combined sensitivity to primordial CMB anisotropies (after foreground removal): **2.2 μK·arcmin**

Hazumi+ SPIE 2020

LiteBIRD cryogenic system

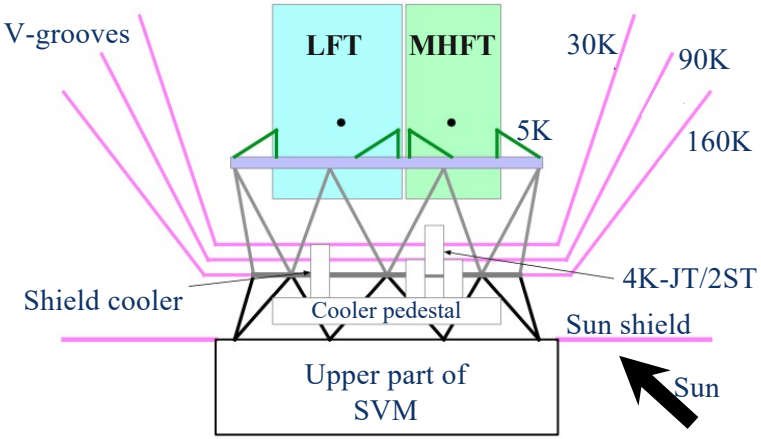

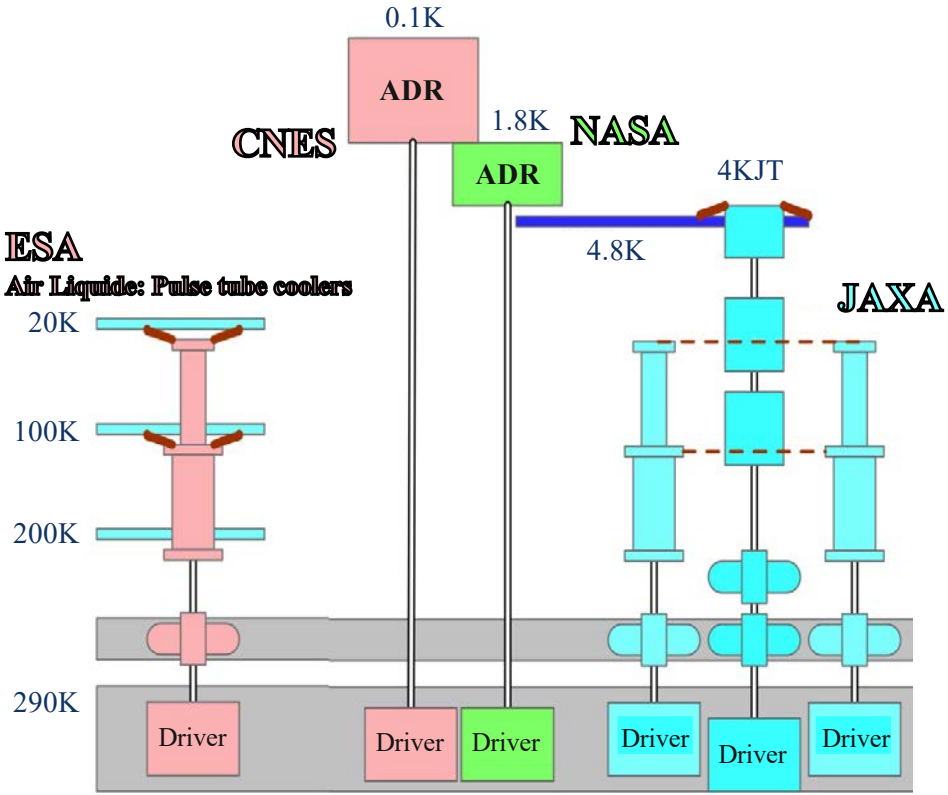

LiteBIRD readout system

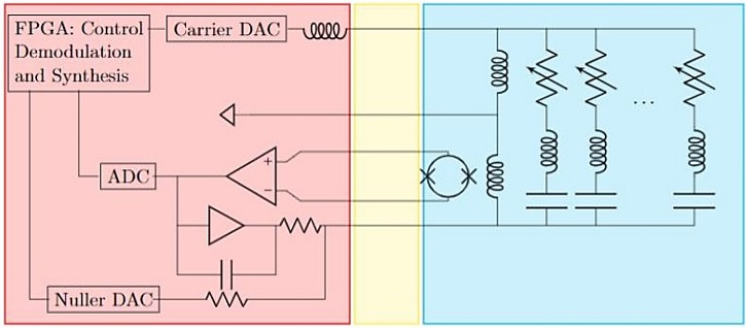

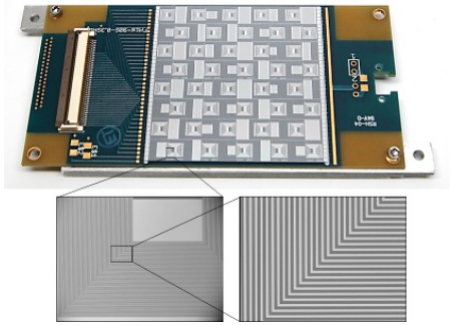

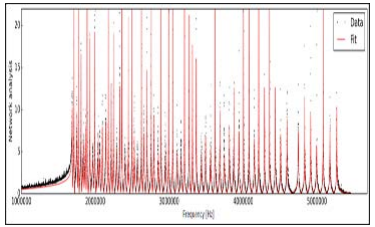

Cold Readout LC filters for MUX

- Frequency multiplexing readout technology to readout multiple TES with less components
- Assign unique frequency channel to TES sensors via superconducting resonators
- Low noise SQUID amplifier and FPGA controller readout the signal
- Saves mass, volume, power consumption and cost
- Heritage from ground based CMB experiments

SQUID controller board

SQUID controller assembly

Digitizer assembly

Signal Processing Unit

Digitizer assembly

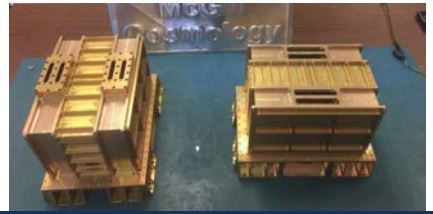

Polarization Modulation Unit (PMU)

- Rotating a birefringent plate to modulate polarization
- The first sky-side optical element

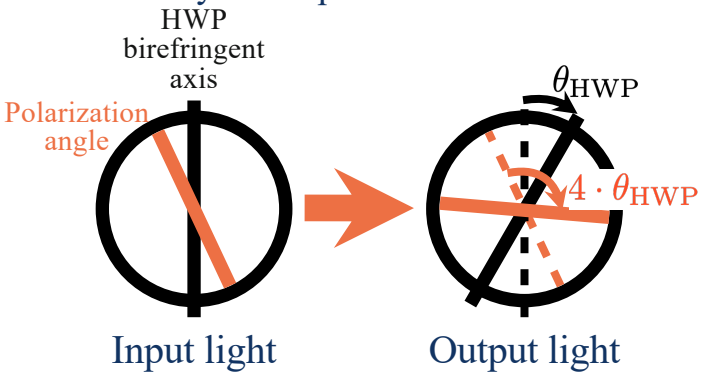

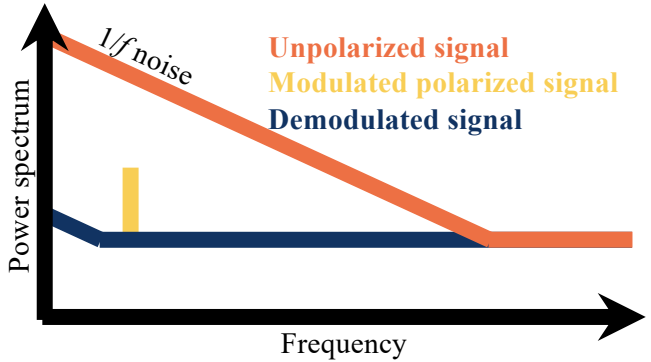

Sakurai+2020 | Komatsu+2020 | Toda+2020 | Columbro+2020 | Sugiyama+2020

- LFT PMU BBM at Kavli IPMU:

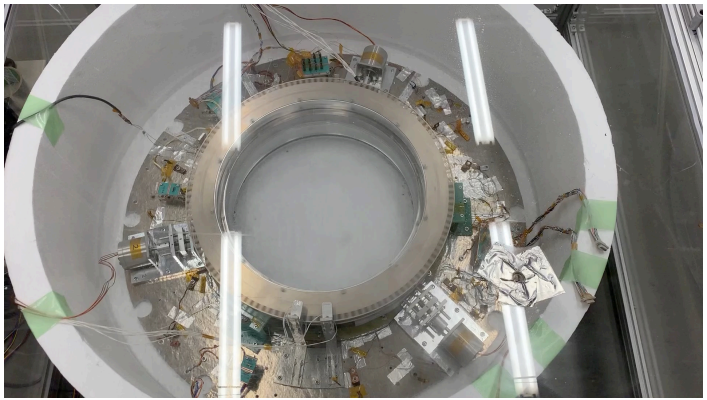

- Rotation test of superconducting magnetic bearing system in the 4K cryostat
- Stable rotation at cryogenic temperature (< 10 K)

Foreground cleaning

Foreground modeling

- **Synchrotron**: curved spectrum (AME is absorbed in the curvature)

$$[Q_{\rm s}, U_{\rm s}]\,(\hat{n}, \nu) = [Q_{\rm s}, U_{\rm s}]\,(\hat{n}, \nu_\star) \cdot \left(\frac{\nu}{\nu_\star}\right)^{\beta_{\rm s}(\hat{n}) + C_{\rm s}(\hat{n})\,\ln(\nu/\nu^{\rm c})}$$

- **Dust**: modified blackbody

$$[Q_{\rm d}, U_{\rm d}]\,(\hat{n}, \nu) = [Q_{\rm d}, U_{\rm d}]\,(\hat{n}, \nu_\star) \cdot \left(\frac{\nu}{\nu_\star}\right)^{\beta_{\rm d}(\hat{n})-2} \frac{B_\nu\,(T_{\rm d}(\hat{n}))}{B_{\nu_\star}\,(T_{\rm d}(\hat{n}))}$$

8 parameters in each sky patch

- "**Multipatch** technique" (extension of xForecast), to account for spatial variability. $12\times(N_{\rm side})^2$ patches ⇒ 6144 parameters with $N_{\rm side} = 8$

Impact of foregrounds residual

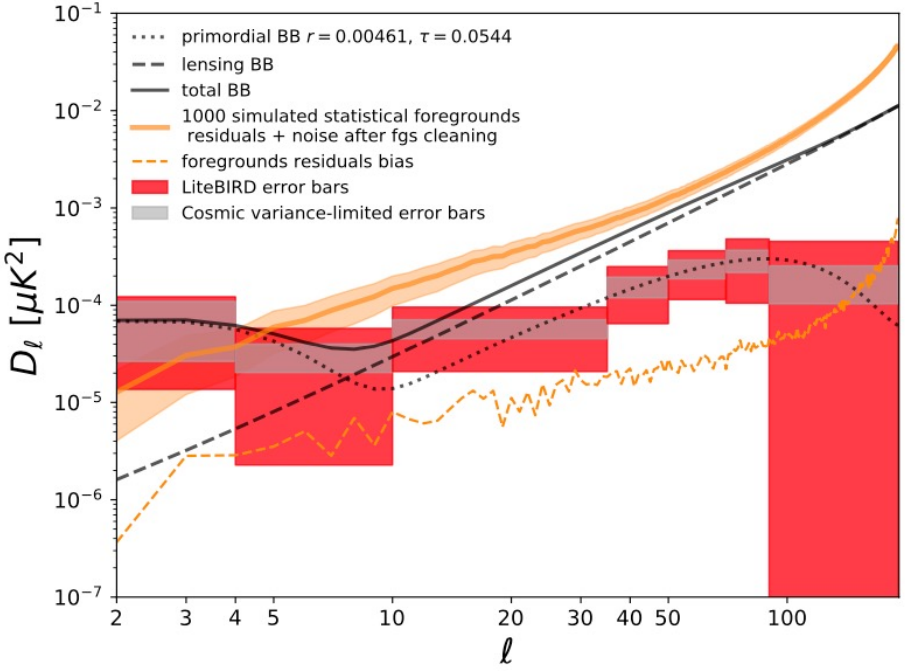

Foreground cleaning

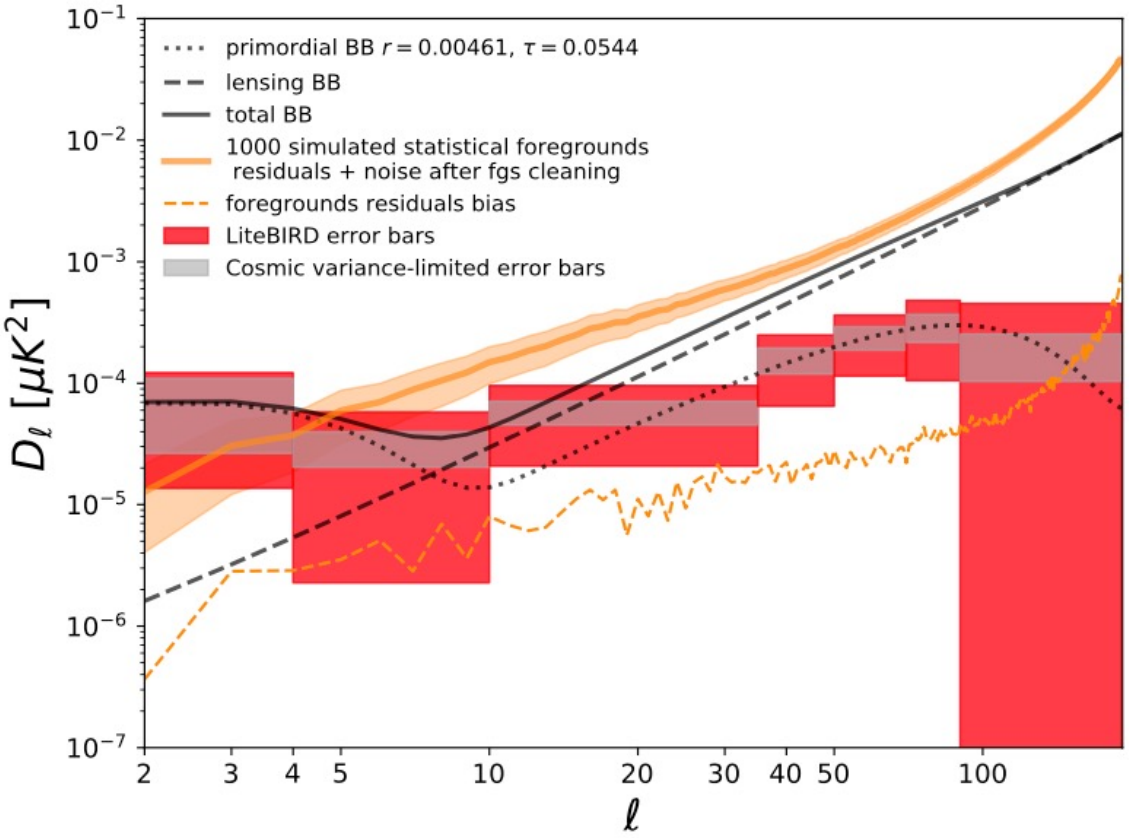

Impact of foregrounds residual

The orange noise and foreground residual can be subtracted

Leaving the orange dashed residual uncertainty

which adds to the cosmic variance uncertainty

to make the red error-bars

Foreground cleaning

- “Multipatch technique” (extension of xForecast)
- Distribution of the recovered r in 1000 simulations with input r=0, with and without foreground residuals
- Bias from foreground residuals is found to be negligibly small
- Final error $\sigma(r=0) = 6\times10^{-4}$

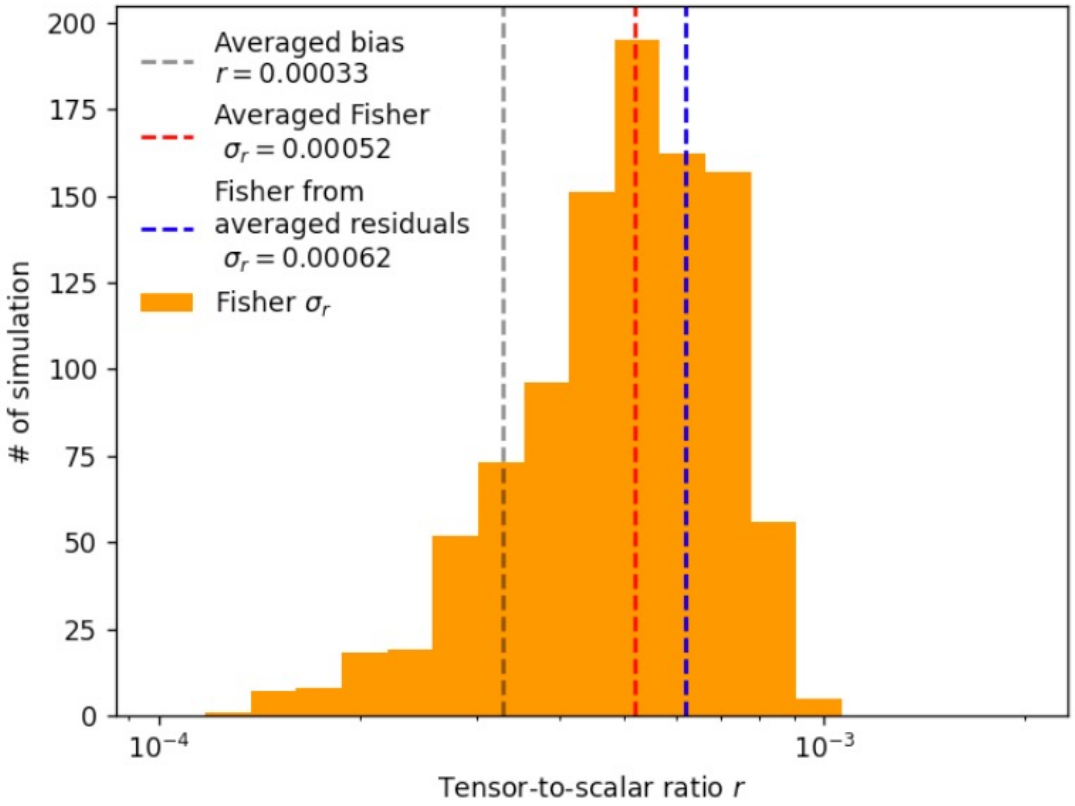

Take-home messages

CMB polarization can reveal primordial gravitational waves, produced during inflationary phase

The GW amplitude is encoded in the B-mode angular power spectrum, by parameter r: tensor-to-scalar ratio

No detection up-to now, only upper limit

More sensitivity is required

Measurements are difficult!

- Sensitivity => large number of detectors and integration time
- Foreground emission => many frequency bands, astrophysical modeling
- Systematic effects => stability, redundancy, Polarization Modulation

Relevant international effort ongoing. Among the others:

- LSPE balloon+ground: δr=0.01, 3 years timescale
- LiteBIRD satellite: δr=0.001, 10 years timescale
- US-ground effort in parallel. 10 years timescale, complementary to LiteBIRD
- Other experiments are ongoing in parallel (QUBIC, QUIJOTE, COSMO, ...)

References

Wayne Hu, CMB statistics: http://background.uchicago.edu/~whu/Courses/Ast448_15/ast448_1.pdf

M. Zaldarriaga & U. Seljak 1997: All-sky analysis of polarization in the microwave background PRD v55 n4

J.M. Lamarre= Photon noise in photometric instruments at far-infrared and submillimeter wavelengths, Appl. Opt. 25, 870-876 (1986)

Planck 2013 results. XVI. Cosmological parameters

Planck 2018 results. VI. Cosmological parameters

Bicep-Keck collaboration. PHYSICAL REVIEW LETTERS 127, 151301 (2021) Improved Constraints on Primordial Gravitational Waves using Planck, WMAP, and BICEP/Keck Observations through the 2018 Observing Season

The LSPE collaboration, The large-scale polarization explorer (LSPE) for CMB measurements: performance forecast, JCAP issue 08 2021

M. Hazumi et al, LiteBIRD satellite: JAXA's new strategic L-class mission for all-sky surveys of cosmic microwave background polarization, Proc. SPIE 11443, Space Telescopes and Instrumentation 2020: Optical, Infrared, and Millimeter Wave, 114432F (21 December 2020)

Y. Sekimoto et al: Concept design of low frequency telescope for CMB B-mode polarization satellite LiteBIRD, Proc. SPIE 11453, Millimeter, Submillimeter, and Far-Infrared Detectors and Instrumentation for Astronomy X, 1145310 (16 December 2020)

L. Lamagna et al: The optical design of the Litebird middle and high frequency telescope, Proc. SPIE 11443, Space Telescopes and Instrumentation 2020: Optical, Infrared, and Millimeter Wave, 1144370 (13 December 2020)

L. Montier et al: Overview of the medium and high frequency telescopes of the LiteBIRD space mission, Proc. SPIE 11443, Space Telescopes and Instrumentation 2020: Optical, Infrared, and Millimeter Wave, 114432G (15 December 2020)

LiteBIRD PTEP 2022 paper (in preparation)